ABSTRACT

ROSS, NATALIE ALEXANDRA. Development and Application of a Continuous-Flow Chamber Technique to Measure Nitrous Oxide Emissions from Agroecosystems in the Southeast (Under the direction of Drs. Wayne Robarge, Chris Reberg-Horton, and Julie Grossman).

Release of nitrous oxide (N_2O) from agricultural soils exhibits temporal and spatial variability, both of which contribute to uncertainty in quantifying cumulative N_2O emissions. The objective of this study was to decrease uncertainty due to temporal variability in cumulative N_2O emissions estimates from agricultural soils. A robust monitoring system was used to record an index of the N_2O temporal emissions curve in a no-till, conventional agroecosystem in the Southeast. Quantitative flux measurements were obtained using non-steady state static chambers. The continuous system operated continuously and unattended in the field, and it used an infrared gas analyzer (Teledyne® Model T320U) and several flow-through chambers interconnected via a set of solenoid valves controlled by a microprocessor. Flow rates were controlled by critical orifices mounted in common manifolds. A laptop computer running DAQ interface (DAQ Plot®, VVI Software) continuously recorded gas concentration and sampling location. Individual chambers (n=4) were sampled for 30-minute intervals. Ambient N_2O was measured every 2 hours. During the study period there was only one peak flux event, during which the bulk of N_2O flux occurred. For the remainder of the season no peak fluxes were observed, though low-levels of N_2O flux were detectable. It is likely that the flux remained low after the peak flux due to drought. Static-chamber flux measurements were made as soon as possible after rain events and for at least three consecutive days thereafter. Individual static-chamber flux measurements were calculated using the best fit of either linear regression or the modified Hutchinson-Mosier (HMR) method. Cumulative flux was estimated three ways, with the first approach using linear

interpolation of the static-chamber flux measurements and integration under the curve (LII). The temporal curve from the continuous system was then used to inform adjustments to the LII approach by defining the start of a flux event (LIIS). For a third approach, N_2O flux decay constants (n=4) were derived from continuous measurements and averaged (RSD = 12.3%). Using the derived decay constant, a simple exponential decay curve was applied to the static chamber measurements in conjunction with the LIIS approach to estimate cumulative flux. The cumulative N_2O flux values from the LII, LIIS, and LIISD methods were 1009 ± 827, 609 ± 379, and 768 ± 540 mg N_2O m^{-2}, respectively. In this study, the LII approach over-estimated the cumulative N_2O flux as revealed by the temporal pattern in actual N_2O emissions derived from using the flow-through chambers. Correcting the tendency to over-estimate flux using the LIIS approach by adding in an estimate of the start in enhanced N_2O emissions led to an inherent underestimation in flux because of the time lag between the start in enhanced N_2O emissions and the actual peak in N_2O emissions. This tendency to underestimate cumulative flux using the LIIS approach was corrected with the LIISD approach by approximating the area under curve following the exponential decline after the peak in N_2O emissions. Improvements in flow-through chamber design will continue with incorporation of automated, flow-through chambers into the continuous system.

Development and Application of a Continuous-Flow Chamber Technique to Measure Nitrous Oxide Emissions from Agroecosystems in the Southeast

by
Natalie Alexandra Ross

A thesis submitted to the Graduate Faculty of
North Carolina State University
in partial fulfillment of the
requirements for the degree of
Master of Science

Soil Science

Raleigh, North Carolina

2016

APPROVED BY:

_____	_____
Dr. Wayne Robarge	Dr. Julie Grossman
Committee Co-Chair	Committee Co-Chair

_____
Dr. Chris Reberg-Horton

DEDICATION

This work is dedicated to all those who seek a deeper understanding of our world and how we are connected to everything in it.

BIOGRAPHY

Natalie Ross is an explorer of the world through both science and art. She came to science by way of an article about mycologist Paul Stamets. The article shared how a simple oyster mushroom (*Pleurotus ostreatus*) could transform toxic, diesel-contaminated soil into a thriving ecosystem, while other remediation efforts of the same soil showed poor to no results. This simple demonstration of the power of fungi and soil inspired the eternal free spirit, Natalie, to study our natural world in a formal way. Lucky for her, NCSU was practically in her backyard and the price was right. Thus, over a decade after starting her undergraduate career (and after dropping out UNC twice – once to move to San Francisco and the other time to move to NYC) she graduated from NCSU and loved her alma mater so much that she decided to stay at NCSU to study soils in a graduate program. Now she's emerged from her master's program, like a butterfly from a cocoon, into the "real world" with a pocketful of science and a heart full of art. She intends to combine her knowledge of agriculture with her technology and communication skills to bring the stories of small, local farmers to the public in a big way. If for some crazy reason you want to talk to her, she can be summoned by sending a message on the wind. If you don't know how to do that, then a singing telegram will suffice.

ACKNOWLEDGMENTS

First and foremost I extend my gratitude to Dr. Wayne Robarge for his patient guidance through this research and writing experience! I've enjoyed working with Dr. Robarge more than I can describe with words. Thank you Dr. Julie Grossman for opening the door to this research for me and to Dr. Chris Reberg-Horton for keeping the door open.

Of course none of this would have happened without the loving support of my family, including, but not limited to, my husband, Dr. John Jack, my parents and stepparents, my sisters, my grandparents and my extended and in-law families. I am so grateful to all of you for encouragement!

Thank you to all the staff at CEFS who patiently and willingly lent a hand and dealt with our unconventional field instrumentation. You all rock!

And finally thank you to all the hard-working scientists who paved the way for this research. Together we make science move forward, one small step at a time.

TABLE OF CONTENTS

LIST OF TABLES

LIST OF FIGURES

CHAPTER 1

Throughout Earth's 4.5 billion-year history, average global temperatures have fluctuated. For at least the last 500,000 years the earth has experienced periods of warming and cooling, called interglacial and glacial periods, respectively, which occur cyclically (American Association for the Advancement of Science, 2009; Fletcher, 2013). Approximately every 100,000 years the glacial period is interrupted by a prolonged interglacial period that lasts approximately 15,000 to 20,000 years. Approximately 10,000 years ago the earth entered an interglacial period called the Holocene epoch, which ushered in the rise of agriculture. While the natural processes of climate change continued, agriculture introduced new anthropogenic effects on the atmosphere and the climate that continue into the present day.

Global warming, or an increase in the average global temperature, is a natural part of an interglacial period. The main driver of global warming is radiative forcing, or an imposed change in the balance between the energy earth receives from the sun and the energy that radiates back into space (IPCC, 2007). Global warming creates changes in average long-term weather patterns over various regions, which is climate change. Prior to 1750 AD, radiative forcing occurred mainly as a result of natural causes (IPCC, 2007). Since pre-industrial times (1750 AD), anthropogenic causes have increased radiative forcing by approximately 2.3 W/m^2 (IPCC, 2014). From 1880 to 2012 the average land and ocean surface temperature increased approximately 0.85 °C (IPCC, 2014).

Evidence overwhelmingly suggests that the cause of global warming is anthropogenic (USEPA, 2013; IPCC, 2014), and scientific societies, including the Soil Science Society of

America, agree that the earth's temperature increase is mainly the result of an increase in anthropogenic greenhouse gas emissions since 1750 AD (American Association for the Advancement of Science, 2009).

Greenhouse Gases

The major natural and anthropogenic greenhouse gases are water vapor (H_2O), carbon dioxide (CO_2), methane (CH_4), nitrous oxide (N_2O), ozone (O_3), and chlorofluorocarbons (CFCs) (USEPA, 2013). Water vapor, clouds and CO_2 account for 95% of the total greenhouse effect (Schmidt et al., 2010).

The greatest source of anthropogenic radiative forcing is CO_2. The atmospheric residence of CO_2 is 10s to 1000s of years, and it is being released into the atmosphere at a greater rate than any other greenhouse gas (Schmidt et al., 2010; Fletcher, 2013). However, CH_4 and N_2O are also important greenhouse gases, having approximately 28 and 300 times, respectively, the global warming potential of CO_2 over a 100-year period (USEPA, 2013; IPCC, 2014).

Land use change and the burning of fossil fuels are the greatest anthropogenic sources of greenhouse gas emissions worldwide (IPCC, 2007; Fletcher, 2013). Deforestation, industrial processes, agriculture, and anaerobic microbial respiration of organic matter in landfills are also important sources of emissions.

Opportunities for mitigation of greenhouse gases are present in many industries. Increasing the use of renewable energy sources such as solar and wind power in industrial and home settings and increasing energy efficiency in automobiles are some of the first steps

to mitigating anthropogenically induced global warming. Agriculture also presents opportunities for mitigation of multiple greenhouse gases, including N_2O.

Nitrous Oxide

N_2O is a greenhouse gas with an atmospheric lifetime of 114 years (IPCC, 2007) and roughly 300 times the global warming potential of CO_2 over a 100-year period (USEPA, 2013). Chemical transformations of N_2O in the stratosphere lead to production of NO and NO_2, which are ozone depleting gases (IPCC, 2007; Ravishankara et al., 2009). Based on direct observations and model predictions, the atmospheric concentration of N_2O in 2005 was estimated to be 319 ± 0.12 ppb, which is well above the estimated pre-industrial range of 180-260 ppb (IPCC, 2007). Since 1750 AD, N_2O atmospheric concentrations have risen ~18% (IPCC, 2007; USEPA, 2013), and the current rate of N_2O increase in the atmosphere is 0.25% yr^{-1} (IPCC, 2007). It is estimated that 4.1-8.1% of the anthropogenic greenhouse effect can be attributed to N_2O (Mosier et al., 1998; IPCC, 2007).

The primary natural and anthropogenic sources of N_2O release into the atmosphere include the manufacturing of nylon; burning of plant-derived materials; atmospheric oxidation of ammonia; emissions from river, estuarine and ocean ecosystems; and the microbial processes of nitrification (NTR), denitrification (DNF) and nitrifier denitrification in soil ecosystems (Bateman and Baggs, 2005; IPCC, 2007). The greatest amount of N_2O emitted from soils comes from 0° to 30° N of the equator (Hirsch et al., 2006).

Agricultural Nitrous Oxide Emissions

Nitrification and Denitrification

Aerobic NTR and anaerobic DNF in agricultural soils are the most significant anthropogenic sources of N_2O (IPCC, 2007; Reay et al., 2012), with cropland soils accounting for 64% of direct annual anthropogenic release of N_2O into the atmosphere (USEPA, 2013). NTR is the aerobic microbial transformation of ammonium into nitrogen (N) oxides (NO_3^- and NO_2^-) (Thangarajan et al., 2013). DNF is an anaerobic stepwise process during which microbes respire N-oxides to nitric oxide (NO), N_2O and dinitrogen gas (N_2) (Philippot et al., 2007; Felber et al., 2012; Senbayram et al., 2012).

DNF requires limited O_2 availability, NO_3^- and NO_2^-, electron donors from organic carbon (C) compounds, and microorganisms capable of DNF (Philippot et al., 2007). Anaerobic conditions are most often induced by precipitation or irrigation events filling the soil pore space with water. Fertilizers, NTR and soil organic matter provide a supply of NO_3^- and NO_2^-, and in the case of organic fertilizers, a source of organic C.

Natural factors that influence soil N_2O emission rates include soil texture, pore structure and aeration, NO_3^- and NO_2^- availability, soluble C, pH, moisture, and temperature (Avrahami et al., 2002; Philippot et al., 2007; Baggs et al., 2010). Wetting-drying events and freeze-thaw cycles also influence production and emissions of N_2O from soils (Sehy et al., 2003; Dilly et al., 2011).

Management Effects on Emissions

The main management-related factors that affect N_2O emissions are tillage and fertilizer source, synchrony and rate (Philippot et al., 2007; Venterea et al., 2011). Tillage

effects on soil N_2O emissions are not clearly articulated in the literature. Grandy et al. (2006) found no significant difference in N_2O emissions between conventional-till (CT) and no-till (NT) systems over six years of corn production in southwestern Michigan. Smith et al. (2012) found no difference in cumulative N_2O flux from CT and NT fields growing corn in northeast Alabama. In a 3-year study in Nashville, TN, average cumulative N_2O emissions were higher in CT than in NT (0.48 and 0.29 mg m^{-2} h^{-1}, respectively) (Deng et al., 2015). Venterea et al. (2011) found no difference in area-scaled N_2O emissions between CT and NT during three corn growing seasons in Minnesota. However, when N_2O was expressed per unit yield of grain, emissions were 52% greater in NT than in CT.

Type of N applied can affect the physical and chemical properties of the soil (Mulvaney et al., 1997), thus influencing the potential for DNF to occur. Timing of N application to synchronize with crop uptake can reduce N_2O emissions, due to there being less N substrate available for DNF (Millar et al., 2010). Cardenas et al. (2010) observed a linear increase in cumulative emissions with N application rates up to 150 kg ha^{-1}, after which cumulative emissions increased exponentially with N rate.

Modeling Nitrous Oxide Emissions

Models are necessary for extrapolating measured N_2O emissions data across larger spatial and temporal scales. They allow for estimates of N_2O emissions when direct measurement is not an option. Models can also predict potential impacts of management on greenhouse gas emissions. The most often used models for estimating N_2O emissions from soils are the DeNitrification DeComposition model (DNDC), the DayCent model, and the emission factor model.

DeNitrification DeComposition Model

The DNDC model is a process-based model that simulates C and N cycling and accounts for environmental and management parameters in estimating and simulating N_2O emissions (Gilhespy et al., 2014; Uzoma et al., 2015). The original DNDC model started as a way to simulate N_2O emissions from agricultural soils in the US. It has been modified over the past two decades to work with many ecosystems, including wetlands and forests. The DNDC model can help pinpoint where the bulk of emissions are occurring in a region, allowing for strategic, directed mitigation.

In the DNDC model ecological drivers of trace gas emissions are linked to soil environmental variables, which are then linked to trace gas production through nitrification, denitrification and fermentation. The three main driving factors of N_2O production or consumption in the DNDC model are soil redox potential (Eh), dissolved organic C (DOC) concentration, and labile N concentration (Giltrap et al., 2010). DNDC can predict both nitrification and denitrification at the same time using the 'anaerobic balloon' concept (Giltrap et al., 2010; Gilhespy et al., 2014). The anaerobic balloon consists of anaerobic microsites that expand or shrink based on the redox potential of the soil.

While they did not compare cumulative N_2O emissions between the DNDC estimates and static chamber measurements, Deng et al. (2016) observed that the DNDC model was able to accurately predict both the timing and magnitude of temporal variations in N_2O emissions over three cropping seasons in Nashville, TN. In a study comparing DNDC N_2O estimates to continuous measurement data in a poorly drained Dystric Vertisol soil, Uzoma et al. (2015) reported that the model underestimated emissions over a 7-year period by 11%.

This is in part likely due to the inability of the DNDC hydrology framework to account for water flow during periods of high rainfall. The DNDC model continues to be modified for worldwide applications.

DayCent Model

DayCent is a process-based model used to estimate N_2O emissions in the annual Environmental Protection Agency (EPA) report to the United Nations Framework Convention on Climate Change (UNFCCC). DayCent is similar to DNDC in that it uses submodels controlled by nutrient inputs, management activities, and climate conditions to simulate greenhouse emissions (Scheer et al., 2014).

In a two-year study growing wheat and cotton in Australia, DayCent accurately predicted the timing and magnitude of emissions from fertilizer additions to cotton (Scheer et al., 2014). DAYCENT predictions of cumulative N_2O emissions were within 16% of measured values from Kentucky bluegrass and ryegrass lawns in Colorado (Zhang et al., 2013). DayCent predictions compared to measured data in an Irish sandy clay loam pasture suggested that applied N remaining in the soil horizon was sufficient to generate a second peak in N_2O emissions in late summer, however no such peak was observed (Abdalla et al., 2010). Except for this overestimate, the model-generated cumulative flux only deviated by 1% from the measured flux. In this same study, DayCent provided a better fit than DNDC for the cumulative N_2O fluxes from both wheat and cotton.

Emission Factor Model

The emission factor model is used by the Intergovernmental Panel on Climate Change (IPCC) to estimate countrywide N_2O emissions. Evidence suggests that N application rate is the most important factor for predicting N_2O emissions when comparing N source, application method, rate and timing. Numerous studies agree that N_2O cumulative emissions linearly increase with N rate, giving rise to the emission factor model used in the IPCC Tier 1 approach (Millar et al., 2010). The IPCC has set a default Tier 1 soil N_2O emission factor of 1%, meaning that 1% of inorganic N made available in soils by human activity is lost as N_2O.

In an analysis examining the quality of data used to develop the default IPCC soil N_2O emission factor, Rochette and Eriksen-Hamel (2008) found very low confidence levels in 50% of N_2O flux reports. They also found that while the reported data might be useful for comparisons between treatments within a study, the experimental bias limited comparison of fluxes between studies. The IPCC default 1% emission factor is not always in agreement with measured emission factors. In a 2-year, static-chamber method study Cardenas et al. (2010) observed that N_2O emissions increased exponentially, rather than linearly, with N rate, giving rise to emission factor values both lower and higher than 1%.

Measuring Nitrous Oxide Emissions from Soils

Calculating cumulative N_2O flux from an agro-ecosystem involves measuring N_2O emissions from the soil several times during a study period, interpolating between flux measurements and then integrating under the curve to generate the cumulative flux value. No single method of measuring N_2O flux from the soil-to-atmosphere interface has been

established as the official standard because methods cannot be calibrated in an absolute manner. The two main categories of methods used for measuring soil N_2O flux are the chamber and micrometeorological techniques. Each has its advantages and disadvantages, and the use of either method depends on the objectives of the study.

Micrometeorological Techniques

With micrometeorological techniques, fluxes are measured from a large footprint without disturbing the soil ecosystem using tower-based instrumentation (Uzoma et al., 2015). These techniques are ideal for measuring and integrating trace gas flux over areas of 0.01-1.0 km^2 (Laville et al., 1999). They do not work as well for smaller source areas or for assessing flux over a relatively short distances, such as plot-based designs that are typical in agricultural studies. The main sources of error in measuring N_2O flux with micrometeorological techniques are due to the high spatial and temporal variability of N_2O soil emissions (Nicolini et al., 2013). Micrometeorological techniques are also the most expensive method for measuring N_2O flux.

Comparisons of micrometeorological and chamber-based N_2O flux measurements present both agreement and disagreement between measured values (Nicolini et al., 2013), with greater agreement occurring when the flux sources were well represented by both methods. Micrometeorological techniques are difficult to replicate, which gives preference to using chambers to quantify N_2O flux measurements in replicated, plot-based field experiments (Chadwick et al., 2014).

Chamber Techniques

Chamber-based techniques for measuring flux at the soil-to-atmosphere interface include non-flow-through (static) chambers and flow-through (dynamic or continuous) chambers. Regardless of chamber type, the chamber footprint area is typically less than 1 m^2.

Static chamber-based flux methodology is the least expensive option and the most commonly used method for measuring soil N_2O emissions (Parkin and Venterea, 2010). This method relies on diffusion transport of N_2O from the soil pores to the headspace inside the chamber. In the static chamber approach, a chamber anchor is inserted into the soil, and an airtight chamber lid with a septum is placed on the anchor. During chamber closure, gas is extracted multiple times and stored in syringes or pre-evacuated glass vials for lab analysis on a gas chromatograph (GC). Individual static-chamber fluxes are measured by calculating the rate of change of trace gas concentration during chamber deployment time over the area that the chamber covers. Then cumulative flux is estimated by interpolating between individual flux measurements over time and integrating under the curve.

Continuous chambers are similar to static chambers in that they include an anchor inserted into the soil and a chamber lid placed over the anchor during chamber deployment. In continuous chambers air is constantly flowing through the chamber headspace, and the flux is calculated based on mass balance by taking the difference in N_2O concentrations at the inlet and the outlet over time. Inlet and outlet N_2O concentrations are often determined using on-site instrumentation such as an infrared gas analyzer housed in a trailer. With flow-through chambers, cumulative flux is calculated the same way as with the static-chamber

method: by interpolating between individual flux measurements and integrating under the curve for a total cumulative flux value.

For both static and continuous chamber techniques, chamber lids can be placed on the anchors either manually or using an automated system. While manual chamber closure is the least expensive and most widely used option, automatic chamber closure in conjunction with a continuous system provides greater temporal resolution of soil N_2O emissions (Parkin, 2008), while potentially reducing environmental artifacts created by keeping a chamber lid in place for long periods of time. Measuring N_2O flux using automated chamber closure has been accomplished through three main means: using a cover that slides into place over the anchor (Ambus and Robertson, 1998), using a lid that swings up and rests at a 90° angle in standby mode (Breuer et al., 2000; Denmead et al., 2010), and through using a rotary arm that moves the chamber lid onto or off of the anchor (Fassbinder et al., 2013). The use of automated chamber enclosures requires a reliable power source using a permanent power line, a generator, or a simple solar-power system on site.

Static Chamber Flux Calculation Methods

Before cumulative flux can be estimated, flux from individual static chamber measurements must be calculated. The method of calculating flux collected from a single static chamber measurement introduces a large source of possible uncertainty, and there is no single recommended best flux calculation method. Selection of a flux calculation method is based on several factors including number and spacing of measurements in time, auxiliary data available, and the calculated mean square error (MSE) for a given technique. The MSE

provides a method for minimizing both bias and variance (Eq. 1) (de Klein and Harvey, 2015):

$$MSE = Variance + Bias^2 \quad (1)$$

Often a combination of flux calculation methods will provide the least error for a given dataset. In addition to linear regression, there are 5 main methods of flux calculation (de Klein and Harvey, 2015): Hutchinson and Mosier (HM), quadratic regression (QR), non-steady state diffusive flux estimator (NDFE), the modified Hutchinson and Mosier method (HMR), and the chamber bias correction method (CBC). Each method calculates flux from one set of static chamber measurements at a time.

When used with curvilinear data, linear regression tends to underestimate flux. However, it is historically one of the most widely used flux calculation methods because of its simplicity and ease of use. The HM method (Hutchinson and Mosier, 1981) requires exactly three equally timed measurements, and it is not recommended because of improvements upon the method that reduce imprecision. The HMR method (Pedersen et al., 2010) is a modification of the HM method, with the added consideration for lateral gas transport beneath the chambers. It requires 4 or more sampling points, and is available as an R software package that calculates flux with both the HMR and linear regression methods. The HMR software also provides an estimate of the MSE and allows users to manually select linear regression or HMR as the best fit for each set of chamber measurements. The QR method (Wagner et al., 1997) requires at least 3 sampling time points, with no restriction on the spacing of the measurements. It is less biased than linear regression for convex-downward curvature, yet it is more biased in regards to this curvature than other non-linear

methods. The NDFE method (Livingston et al., 2006) is recommended for 4 or more time points. It provides an estimate of flux at time 0, yet it is not recommended for use with large data sets. Further, it can give unexpectedly high flux values and possibly deliver more than one flux value for the same data set when calculated multiple times. The CBC method (Venterea, 2010) first determines flux using a linear regression, HM, or QR, which is then multiplied by a correction factor. It requires soil bulk density, temperature, clay content and water content data, and can be used with 3 or 4 sampling time points.

Cumulative Flux Calculation

Regardless of whether a micrometeorological, static chamber or flow-through chamber technique is used to measure flux from the soil to atmosphere interface, cumulative flux is most often estimated using the trapezoid, or linear, method of interpolating between individual flux measurements and then integrating under the curve. Both over and underestimation of cumulative flux can occur, depending on how aligned or misaligned individual flux measurements are with capturing peak flux events.

Few studies that assess addressing N_2O temporal variability in a static-chamber sampling protocol exist. Parkin (2008) used an automated, continuous system to measure N_2O flux every 6 hours for 8 months to obtain a "true" cumulative N_2O flux estimate. He then subsampled the data to evaluate how static-chamber sampling frequency affected the cumulative N_2O estimates. When sampling at 14-day intervals, cumulative emissions estimates were between -43 and 64% of the "true" cumulative estimate. A cumulative flux estimate within ±10% of the "true" value was obtained by measuring flux every 3 days. The Nitrous Oxide Chamber Methodology Guidelines (NOCMG) (de Klein and Harvey, 2015)

recommends implementing a sampling protocol that addresses the temporal variation of the N_2O source based on when emissions peaks are expected (de Klein and Harvey, 2015).

Standardization of the Static Chamber Method

While no standard method exists for measuring N_2O from soils, the static chamber method with manual chamber lid placement is the *de facto* standard because of its ease of use and low cost. It is a very common method, and there are as many ways to implement it as there are researchers using it. While the method allows comparisons between treatments within a study, the differences between how researchers implement the static chamber method inhibit cross-study comparisons of results due to biases. Therefore the USDA Agricultural Research Service (ARS) has attempted to standardize the static chamber method protocols in a project called GRACEnet. The GRACEnet protocol aims to facilitate the widespread adoption of a common methodology to aid in site inter-comparisons (Parkin and Venterea, 2010). The protocol is being utilized across the United States and is a *best guess* effort to optimize sensitivity, limit bias and variance, and allow accurate interpolation and extrapolation over space and time, despite the inability to precisely assess the extent of bias associated with any given design. As the protocol is relatively new, the effectiveness of the GRACEnet protocol in aiding site inter-comparisons has yet to be determined.

The NOCMG (de Klein and Harvey, 2015) is a collaboration between international N_2O researchers that aims to standardize the methods for measuring agricultural N_2O emissions using chamber techniques and improve inter-comparability between findings of international studies. The document details recommendations for the key aspects of chamber methodology, and it outlines the agreed minimum standards, site or system specific

requirements and evolving standards for each of the key aspects. The key aspects that the NOCMG covers include chamber design, deployment, air sample collection, storage and sample analysis, data analysis and data reporting. Despite their efforts, the NOCMG authors faced difficulty in reducing uncertainty in cumulative emissions estimates due to spatial and temporal variability.

Spatial and Temporal Variability

The GRACEnet protocol and the NOCMG take into account several variables that can affect N_2O flux measurements including soil disturbance, perturbations in temperature, pressure and humidity, gas mixing, chamber placement, frequency and timing of measurements, spatial variation, and method of flux calculation. However, despite these efforts to optimize and standardize the static chamber technique, minimizing bias due to spatial and temporal variability remains a difficulty. This is due to the labor-intensive demands of the technique coupled with the fact that spatial and temporal patterns N_2O emissions are not fixed like a defined soil property.

Spatial variability of emissions is extremely high and has the potential to introduce uncertainty in flux estimates (Chadwick et al., 2014). Reported relative standard deviations (RSD) of spatial variability from static-chamber based measurements ranges from 18% to 397% (Smith and Dobbie, 2001). In a study using static chambers to measure N_2O flux over 15,360 m^2 of grazed and mowed grasslands, Velthof et al. (1996) estimated that 375 to 1240 chambers were needed to measure flux within 10% of the true mean. GRACEnet and NOCMG recommend sampling a minimum of 2 and 3 chambers per plot, respectively, to account for spatial variability (Parkin and Venterea, 2010; de Klein and Harvey, 2015).

The temporal pattern of N_2O flux is driven by soil C and N dynamics, and it is heavily influenced by factors that occur cyclically, such as diurnal and seasonal temperature fluctuations, as well as by factors that occur irregularly, such as rainfall and N application (de Klein and Harvey, 2015). Accounting for temporal variability when measuring N_2O flux from soils reduces uncertainty and provides data that is useful for improving models. This allows greater precision in estimating N_2O flux over areas of all sizes, and assists in developing plans for targeted mitigation in areas and at times with the greatest flux. Since characterizing the temporal pattern of N_2O emissions with the static chamber method is logistically unrealistic, researchers predict when peak flux events are most likely to occur and then focus on sampling heavily around those times. Wetting events create anaerobic conditions in soils that stimulate N_2O production. Thus to account for precipitation-induced emissions, static-chamber sampling typically occurs once between 12 to 72 hours after the end of a wetting event. To account for management-induced N_2O emissions, sampling frequency will often be increased following a management event until emissions return to baseline levels. During times when peak emissions are not expected, sampling will typically occur on an arbitrary schedule, such as once per month, or not at all.

Peak N_2O flux can both climax and decay within a matter of hours following a precipitation or management event (Stehfest and Bouwman, 2006; Fassbinder et al., 2013). Unless flux is measured continuously, the timing and magnitude of the N_2O emissions are unknown (Smith and Dobbie, 2001; Parkin, 2008). Despite increased manual sampling frequency, the potential for failing to capture both the peak and decay of a flux remains. Failure to establish baseline emissions before a peak flux event can introduce uncertainty and

lead to overestimation of cumulative emissions (de Klein and Harvey, 2015). Further, failure to measure flux during an unexpected peak flux event can introduce bias in cumulative N_2O flux estimates (Smith and Dobbie, 2001; Parkin, 2008; Parkin and Venterea, 2010; de Klein and Harvey, 2015).

Objective

Without knowing the pattern and magnitude of N_2O emissions over time, uncertainties due to temporal variability remain, thus contributing to uncertainty in estimating cumulative emissions (Smith and Dobbie, 2001; Parkin, 2008; Reeves and Wang, 2015). Our objective was to reduce uncertainty in cumulative N_2O flux estimates due to temporal variability. We created a continuous flow-through chamber system to monitor the temporal emissions curve and provide an index of the pattern and magnitude of N_2O emissions throughout the growing season. Static chamber measurements were used to quantify N_2O flux based on recommendations from both the GRACEnet and NOCMG protocols. The continuous index was used as a guide for adjusting cumulative emissions estimates from static-chamber measurements by identifying both the occurrence and the beginning of flux events, timing and relative magnitude of the peak, and decay of flux following the peak. The continuous flow-through system was deployed during in a no-till conventional field at the Center for Environmental Farming Systems (CEFS) in Goldsboro, NC, from April until September 2015.

References

Abdalla, M., Jones, M., Yeluripati, J., Smith, P., Burke, J., Williams, M., 2010. Testing DayCent and DNDC model simulations of N2O fluxes and assessing the impacts of climate change on the gas flux and biomass production from a humid pasture. Atmospheric Environment 44, 2961–2970.

Ambus, P., Robertson, G.P., 1998. Automated Near-Continuous Measurement of Carbon Dioxide and Nitrous Oxide Fluxes from Soil. Soil Science Society of America Journal 62, 394.

American Association for the Advancement of Science, 2009. Climate Change Statement.

Avrahami, S., Conrad, R., Braker, G., 2002. Effect of Soil Ammonium Concentration on N2O Release and on the Community Structure of Ammonia Oxidizers and Denitrifiers. Applied and Environmental Microbiology 68, 5685–5692.

Baggs, E.M., Smales, C.L., Bateman, E.J., 2010. Changing pH shifts the microbial source as well as the magnitude of N2O emission from soil. Biology and Fertility of Soils 46, 793–805.

Bateman, E.J., Baggs, E.M., 2005. Contributions of nitrification and denitrification to N2O emissions from soils at different water-filled pore space. Biology and Fertility of Soils 41, 379–388.

Breuer, L., Papen, H., Butterbach-Bahl, K., 2000. N2O emission from tropical forest soils of Australia. Journal of Geophysical Research 105, 26353.

Cardenas, L.M., Thorman, R., Ashlee, N., Butler, M., Chadwick, D., Chambers, B., Cuttle, S., Donovan, N., Kingston, H., Lane, S., Dhanoa, M.S., Scholefield, D., 2010. Quantifying annual N2O emission fluxes from grazed grassland under a range of inorganic fertiliser nitrogen inputs. Agriculture, Ecosystems and Environment 136, 218–226.

Chadwick, D.R., Cardenas, L., Misselbrook, T.H., Smith, K. a., Rees, R.M., Watson, C.J., McGeough, K.L., Williams, J.R., Cloy, J.M., Thorman, R.E., Dhanoa, M.S., 2014. Optimizing chamber methods for measuring nitrous oxide emissions from plot-based agricultural experiments. European Journal of Soil Science 65, 295–307.

de Klein, C., Harvey, M., 2015. Nitrous Oxide Chamber Methodology Guidelines. Ministry for Primary Industries, Wellington, New Zealand.

Deng, Q., Hui, D., Wang, J., Iwuozo, S., Yu, C.-L., Jima, T., Smart, D., Reddy, C., Dennis, S., 2015. Corn Yield and Soil Nitrous Oxide Emission under Different Fertilizer and Soil Management: A Three-Year Field Experiment in Middle Tennessee. Plos One 10.

Deng, Q., Hui, D., Wang, J., Yu, C., Li, C., Reddy, K.C., Dennis, S., 2016. Assessing the impacts of tillage and fertilization management on nitrous oxide emissions in a cornfield using the DNDC model. Journal of Geophysical Research: Biogeosciences 121, 337–

349.

Denmead, O.T., Macdonald, B.C.T., Bryant, G., Naylor, T., Wilson, S., Griffith, D.W.T., Wang, W.J., Salter, B., White, I., Moody, P.W., 2010. Emissions of methane and nitrous oxide from Australian sugarcane soils. Agricultural and Forest Meteorology 150, 748–756.

Dilly, O., Pfeiffer, E.-M., Yanai, Y., Hirota, T., Iwata, Y., Nemoto, M., Nagata, O., Koga, N., 2011. Accumulation of nitrous oxide and depletion of oxygen in seasonally frozen soils in northern Japan – Snow cover manipulation experiments. Soil Biology and Biochemistry 43, 1779–1786.

Fassbinder, J.J., Schultz, N.M., Baker, J.M., Griffis, T.J., 2013. Automated, low-power chamber system for measuring nitrous oxide emissions. Journal of Environmental Quality 42, 606–14.

Felber, R., Conen, F., Flechard, C.R., Neftel, a., 2012. Theoretical and practical limitations of the acetylene inhibition technique to determine total denitrification losses. Biogeosciences 9, 4125–4138.

Fletcher, C., 2013. Climate Change: What The Science Tells Us. Wiley, Hoboken.

Gilhespy, S.L., Anthony, S., Cardenas, L., Chadwick, D., Li, C., Misselbrook, T., Rees, R.M., Salas, W., Sanz-cobena, A., Smith, P., Tilston, E.L., Topp, C.F.E., Vetter, S., Yeluripati, J.B., 2014. First 20 years of DNDC (DeNitrification DeComposition): Model evolution. Ecological Modelling 292, 51–62.

Giltrap, D.L., Li, C., Saggar, S., 2010. DNDC: A process-based model of greenhouse gas fluxes from agricultural soils. Agriculture, Ecosystems and Environment 136, 292–300.

Grandy, A.S., Loecke, T.D., Parr, S., Robertson, G.P., 2006. Long-term trends in nitrous oxide emissions, soil nitrogen, and crop yields of till and no-till cropping systems. Journal of Environmental Quality 35, 1487–1495.

Hirsch, A.I., Michalak, A.M., Bruhwiler, L.M., Peters, W., Dlugokencky, E.J., Tans, P.P., 2006. Inverse modeling estimates of the global nitrous oxide surface flux from 1998-2001. Global Biogeochemical Cycles 20.

Hutchinson, G., Mosier, A., 1981. Improved soil cover method for field measurement of nitrous oxide fluxes. Soil Science Society of America Journal 45, 311–316.

IPCC, 2007. Climate Change 2007: The Physical Science Basis. Contribution of Working Group I to the Fourth Assessment Report of the Intergovernmental Panel on Climate Change. Cambridge University Press, Cambridge, United Kingdom and New York, NY, USA.

IPCC, 2014. Climate Change 2014: Synthesis Report. Contribution of Working Groups I, II and III to the Fifth Assessment Report of the Intergovernmental Panel on Climate Change. IPCC, Geneva, Switzerland.

Laville, P., Jambert, C., Cellier, P., Delmas, R., 1999. Nitrous oxide fluxes from a fertilised maize crop using micrometeorological and chamber methods. Agricultural and Forest Meteorology 96, 19–38.

Livingston, G.P., Hutchinson, G.L., Spartalian, K., 2006. Trace Gas Emission in Chambers. Soil Science Society of America Journal 70, 1459.

Millar, N., Robertson, G.P., Grace, P.R., Gehl, R.J., Hoben, J.P., 2010. Nitrogen fertilizer management for nitrous oxide (N2O) mitigation in intensive corn (Maize) production: An emissions reduction protocol for US Midwest agriculture. Mitigation and Adaptation Strategies for Global Change 57, 185–204.

Mosier, A., Kroeze, C., Nevison, C., Oenema, O., Seitzinger, S., van Cleemput, O., 1998. Closing the global N2O budget: nitrous oxide emissions through the agricultural nitrogen cycle. Nutrient Cycling in Agroecosystems 52, 225–248.

Mulvaney, R.L., Khan, S.A., Mulvaney, C.S., 1997. Nitrogen fertilizers promote denitrification. Biology and Fertility of Soils 24, 211–220.

Nicolini, G., Castaldi, S., Fratini, G., Valentini, R., 2013. A literature overview of micrometeorological CH4 and N2O flux measurements in terrestrial ecosystems. Atmospheric Environment 81, 311–319.

Parkin, T.B., 2008. Effect of sampling frequency on estimates of cumulative nitrous oxide emissions. Journal of Environmental Quality 37, 1390–5.

Parkin, T.B., Venterea, R.T., 2010. Chamber-Based Trace Gas Flux Measurements, in: Follett, R.. (Ed.), Sampling Protocols. pp. 3–1 to 3–39.

Pedersen, A.R., Petersen, S.O., Schelde, K., 2010. A comprehensive approach to soil-atmosphere trace-gas flux estimation with static chambers. European Journal of Soil Science 61, 888–902.

Philippot, L., Hallin, S., Schloter, M., 2007. Ecology of Denitrifying Prokaryotes in Agricultural Soil, in: Advances In Agronomy. Elsevier Inc., pp. 249–305.

Ravishankara, A.R., Daniel, J.S., Portmann, R.W., 2009. Nitrous oxide (N2O): the dominant ozone-depleting substance emitted in the 21st century. Science 326, 123–5.

Reay, D.S., Davidson, E. a., Smith, K. a., Smith, P., Melillo, J.M., Dentener, F., Crutzen, P.J., 2012. Global agriculture and nitrous oxide emissions. Nature Climate Change 2, 410–416.

Reeves, S., Wang, W., 2015. Optimum sampling time and frequency for measuring N2O emissions from a rain-fed cereal cropping system. Science of The Total Environment 530-531, 219–226.

Rochette, P., Eriksen-Hamel, N.S., 2008. Chamber Measurements of Soil Nitrous Oxide Flux: Are Absolute Values Reliable? Soil Science Society of America Journal 72, 331.

Scheer, C., Del Grosso, S.J., Parton, W.J., Rowlings, D.W., Grace, P.R., 2014. Modeling nitrous oxide emissions from irrigated agriculture: Testing DayCent with high-frequency measurements. Ecological Applications 24, 528–538.

Schmidt, G., Ruedy, R., Miller, R.L., Lacis, A., 2010. Attribution of the present-day total greenhouse effect. Journal of Geophysical Research 115.

Sehy, U., Ruser, R., Munch, J.C., 2003. Nitrous oxide fluxes from maize fields: Relationship to yield, site-specific fertilization, and soil conditions. Agriculture, Ecosystems and Environment 99, 97–111.

Senbayram, M., Chen, R., Budai, A., Bakken, L., Dittert, K., 2012. N2O emission and the N2O/(N2O+N2) product ratio of denitrification as controlled by available carbon substrates and nitrate concentrations. Agriculture, Ecosystems and Environment 147, 4–12.

Smith, K. a., Dobbie, K., 2001. The impact of sampling frequency and sampling times on chamber-based measurements of N2O emissions from fertilized soils. Global Change Biology 7, 933–945.

Smith, K., Watts, D., Way, T., Torbert, H., Prior, S., 2012. Impact of Tillage and Fertilizer Application Method on Gas Emissions in a Corn Cropping System. Pedosphere 22, 604–615.

Stehfest, E., Bouwman, L., 2006. N2O and NO emission from agricultural fields and soils under natural vegetation: summarizing available measurement data and modeling of global annual emissions. Nutrient Cycling in Agroecosystems 74, 207–228.

Thangarajan, R., Bolan, N.S., Tian, G., Naidu, R., Kunhikrishnan, A., 2013. Role of organic amendment application on greenhouse gas emission from soil. The Science of the Total Environment 465, 72–96.

USEPA, 2013. Inventory of U.S. Greenhouse Gas Emissions and Sinks: 1990-2011. Washington, DC.

Uzoma, K.C., Smith, W., Grant, B., Desjardins, R.L., Gao, X., Hanis, K., Tenuta, M., Goglio, P., Li, C., 2015. Assessing the effects of agricultural management on nitrous oxide emissions using flux measurements and the DNDC model. Agriculture, Ecosystems & Environment 206, 71–83.

Velthof, G.L., Jarvis, S.C., Stein, a., Allen, a. G., Oenema, O., 1996. Spatial variability of nitrous oxide fluxes in mown and grazed grasslands on a poorly drained clay soil. Soil Biology and Biochemistry 28, 1215–1225.

Venterea, R.T., 2010. Simplified Method for Quantifying Theoretical Underestimation of Chamber-Based Trace Gas Fluxes. Journal of Environmental Quality 39, 126–135.

Venterea, R.T., Bijesh, M., Dolan, M.S., 2011. Fertilizer source and tillage effects on yield-scaled nitrous oxide emissions in a corn cropping system. Journal of Environmental

Quality 40, 1521–31.

Wagner, S.W., Reicosky, D.C., Alessi, R.S., 1997. Regression models for calculating gas fluxes measured with a closed chamber. Agronomy Journal 89, 279–284.

Zhang, Y., Qian, Y., Bremer, D.J., Kaye, J.P., 2013. Simulation of Nitrous Oxide Emissions and Estimation of Global Warming Potential in Turfgrass Systems Using the DAYCENT Model. Journal of Environmental Quality 42, 1100–8.

CHAPTER 2

Introduction

Nitrous oxide (N_2O) is a trace gas with approximately 298 times the global warming potential as carbon dioxide (USEPA, 2013). Globally N_2O accounts for about 5% of the total greenhouse effect (Philippot et al., 2007). Compared to pre-industrial levels, atmospheric concentrations of N_2O have risen about 19% (IPCC, 2007). Nitrous oxide emissions from agricultural soils account for approximately 64% of the total annual anthropogenic U.S. N_2O emissions (USEPA, 2013).

While there is no standard method of measuring soil N_2O emissions, the vented, non-steady state static chamber method is the most widely employed (Parkin and Venterea, 2010). In the static chamber method an anchor is inserted into the soil, and a gas-tight chamber lid with a septum is placed over the anchor for a short period of time. At regular intervals during chamber closure, air samples are extracted from the chamber headspace and injected into gas-tight containers for laboratory analysis (de Klein and Harvey, 2015). This method is relatively inexpensive, easy to transport and use, and works well in smaller plot-size agricultural experiments.

The static chamber method is limited in its ability to address the spatial and temporal variability (Chadwick et al., 2014) of N_2O flux. Flux is the rate of gas exchange between the soil-to-atmosphere interface per area per time. Without a standardized protocol, method-induced bias makes it very difficult to compare N_2O flux data across studies (Rochette and Eriksen-Hamel, 2008). The rate of change of gas in the chamber headspace is not a fixed property, and it is not always constant. Often N_2O builds up in the chamber headspace,

causing flux measurements to be biased low, depending on the flux calculation methods used (Parkin and Venterea, 2010). The GRACEnet protocol (Parkin and Venterea, 2010) offers suggestions to optimize sensitivity, limit bias and variance, and allow accurate interpolation and extrapolation over space and time using the static chamber method. However, GRACEnet's protocols are only a best guess, due to the inability to precisely assess the extent of bias associated with any given design (Parkin and Venterea, 2010).

The method of calculating flux for an event introduces a large source of possible uncertainty. Methods for calculating flux range from simple linear regression to complex methods that require auxiliary data inputs and a specific number of sample points evenly spaced in time. There is no single recommended best method for flux calculation. Selection of a flux calculation method that will best minimize uncertainty is based on several factors including number and spacing of measurements in time, auxiliary data available, and the calculated mean square error (MSE) for a given technique. The MSE provides a method for minimizing both bias and variance (Eq. 1) (de Klein and Harvey, 2015):

$$\text{MSE} = \text{Variance} + \text{Bias}^2 \quad (1)$$

Often a combination of flux calculation methods will provide the least error for a given dataset. In addition to linear regression, there are 5 main methods of flux calculation (de Klein and Harvey, 2015): Hutchinson and Mosier (HM), quadratic regression (QR), non-steady state diffusive flux estimator (NDFE), the modified Hutchinson and Mosier method (HMR), and the chamber bias correction method (CBC). Each method calculates flux for one static chamber at a time. When used with curvilinear data, linear regression tends to underestimate flux. However, it is historically one of the most widely used flux calculation

methods because of its simplicity and ease of use. The HM method (Hutchinson and Mosier, 1981) requires exactly three equally timed measurements, and it is not recommended because of improvements upon the method that reduce imprecision. The QR method (Wagner et al., 1997) requires at least 3 sampling time points, with no restriction on the spacing of the measurements. It is less biased than linear regression for convex-downward curvature, yet it is more biased in regards to this curvature than other non-linear methods. The NDFE method (Livingston et al., 2006) is recommended for 4 or more time points. It provides an estimate of flux at time 0, yet it is not recommended for use with large data sets. Further, it can give unexpectedly high flux values and also possibly deliver more than one flux value for the same data set when calculated multiple times. The HMR method (Pedersen et al., 2010) is a modification of the HM method, with the added consideration for lateral gas transport beneath the chambers. It requires 4 or more sampling points, and is available as an R software package that calculates flux with both the HMR and linear regression methods. The HMR software also provides an estimate of the MSE and allows users to manually select linear regression or HMR as the best fit for each flux value. The CBC method (Venterea, 2010) first determines flux using a linear regression, HM, or QR, which is then multiplied by a correction factor. It requires soil bulk density, temperature, clay content and water content data, and can be used with 3 or 4 sampling time points.

Spatial variability of emissions can exhibit relative standard deviations greater than 100% (Smith and Dobbie, 2001; Parkin, 2008; Parkin and Venterea, 2010). In a study using static chambers to measure N_2O flux over 15,360 m^2 of grazed grassland, (Velthof et al., 1996) it was estimated that 375 to 1240 chambers would have been needed for measurements

to be within 10% of the true mean. A minimum of three chamber replicates per treatment are recommended to reduce spatial variability (de Klein and Harvey, 2015). Consideration of variation in the topography and differences in the field conditions due to management activities should be accounted for when determining criteria for chamber placement. Chambers with a larger footprint can also reduce spatial variability (Parkin and Venterea, 2010). When hotspots are identifiable, such as by visible signs of urine patches (Oenema et al., 1997), a sampling design can be developed to reduce spatial variability due to such hotspots. Increased resolution in the temporal characterization of soil N_2O flux is necessary for assessing and addressing uncertainty due to spatial variation.

Small- and large-scale temporal variations of N_2O emissions can impact cumulative estimates of emissions. Day-to-day magnitudes of emissions can differ substantially (Halvorson and Del Grosso, 2012; Reeves and Wang, 2015), further complicating the ability to estimate cumulative N_2O emissions from static-chamber based data. Fassbinder et al. (2013) observed that weekly static chamber sampling missed peak N_2O fluxes that were recorded by a continuous monitoring system, leading to underestimation of cumulative flux using static chamber data. Identifying key time points when N_2O flux is expected and developing a sampling strategy to capture the flux temporal pattern can potentially address temporal variability when using the static chamber method to estimate cumulative flux.

Denitrification is an anaerobic microbial process that produces N_2O (Galloway, 2003). Wetting events create anaerobic conditions in soils that trigger denitrification. Therefore N_2O sampling typically occurs once between 12 to 72 hours after a wetting event (Fassbinder et al., 2013). Without sampling multiple times before and after a wetting event,

the pattern and magnitude of each temporal emissions curve is unknown, thus leading to possible uncertainties in estimating cumulative emissions (Smith and Dobbie, 2001; Parkin, 2008; Reeves and Wang, 2015). Temporal variability is reduced by more frequent flux measurements (Smith and Dobbie, 2001; Parkin, 2008).

Our objective was to reduce uncertainty in cumulative N_2O flux estimates due to temporal variability. We attempted to use a relatively simple continuous monitoring system to create an index of the temporal N_2O emissions curve, while relying on non-steady state static chamber measurements for quantitative flux measurements. The temporal emissions curve was used to address uncertainties in the static-chamber based estimation of cumulative flux due to temporal variation. While systems for continuously and quantitatively measuring N_2O flux are available, they add cost and complexity, especially for assessing flux in more than 1 or 2 locations. Our system mirrors that created by Fassbinder et al. (2013), with the key difference being that we did not use the continuous system quantitatively, but rather qualitatively to inform static-chamber sampling protocols and the manipulation of results from static-chamber measurements in estimating cumulative emissions.

Materials and Methods

Study Site Location

The research site was situated in the Farming Systems Research Unit (FSRU) at the Center for Environmental Farming Systems (CEFS) near Goldsboro, NC (35°23′N, 78°02′W, elevation 35 m above sea level). The FSRU is an 81-hectare interdisciplinary long-term study of five systems laid out in a randomized complete block design with three replicates. The study site falls in a region that has a humid subtropical climate with a mean annual

temperature of 16.7˚C and precipitation of ~1240 mm yr^{-1} (Arguez et al., 2010). The Neuse River borders CEFS on three sides, creating high spatial variability in soil types within the river basin.

Actual measurements were taken in a subplot of the Best Management Practices (BMP) treatment of the Conventional Cash Cropping System. The BMP has a three-year rotation of corn, soybean and grain sorghum, with winter cover crops used in all three years. The BMP is split into subplots of conventional tillage and no-till. Measurements were restricted to a no-till subplot of the BMP, to allow chamber anchors to remain undisturbed as much as possible, with a corn-soybean rotation that started in spring 2013 and winter cover crops.

Because of the high spatial variability in soil types across the FSRU, the area has been mapped for defined diagnostic soil units via an intensive GPS-based soil survey. The diagnostic, dominant soil in the no-till subplot used in this study is a well-drained Wickham sandy loam (fine-loamy, mixed, semiactive, thermic Typic Hapludult). Average depth to the water table is greater than 200 cm (Soil Survey Staff et al., 2015). Selected soil physical and chemical properties of the 0-30 cm soil depth for the study site are: pH 6.1; bulk density 1.53 g cm^{-3}; 19% clay; 61.7% sand; and 19.4% silt (Soil Survey Staff et al., 2015) (Bell and Raczkowski, 2008).

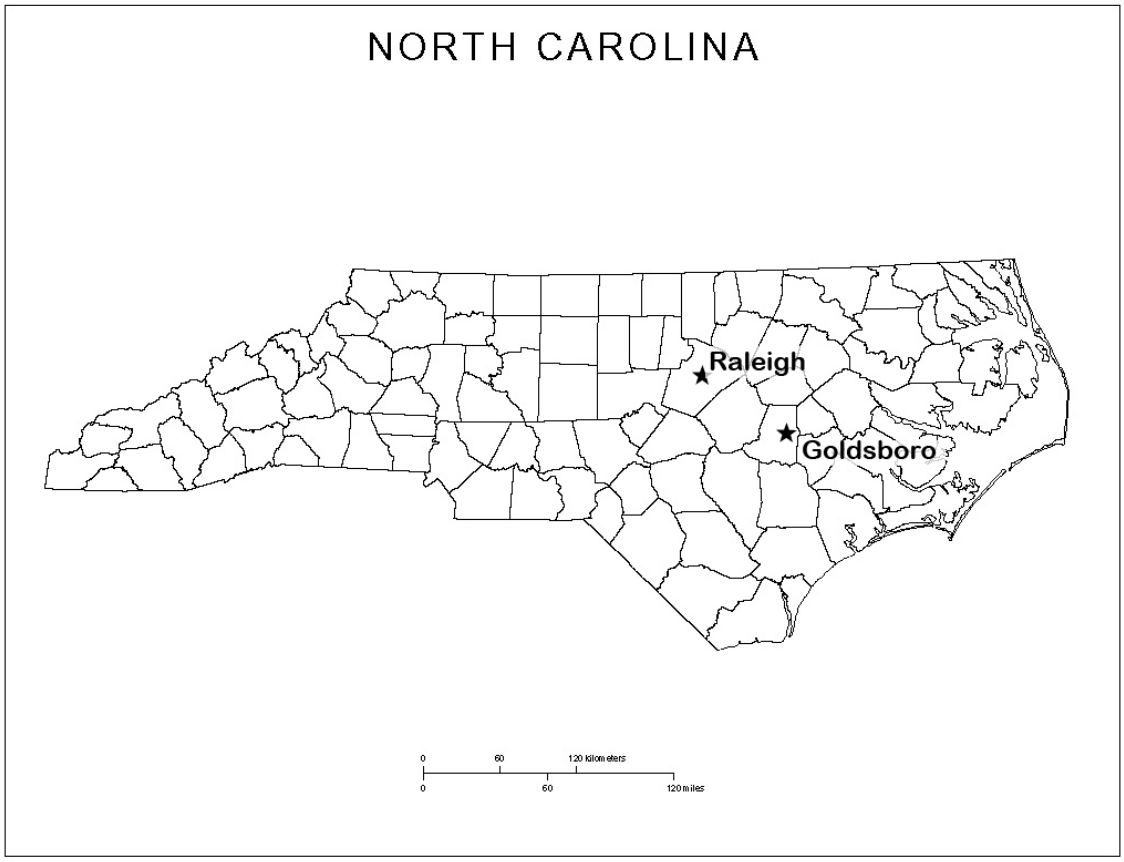

Figure 1. State map of North Carolina showing the location of the study site at Goldsboro, NC.

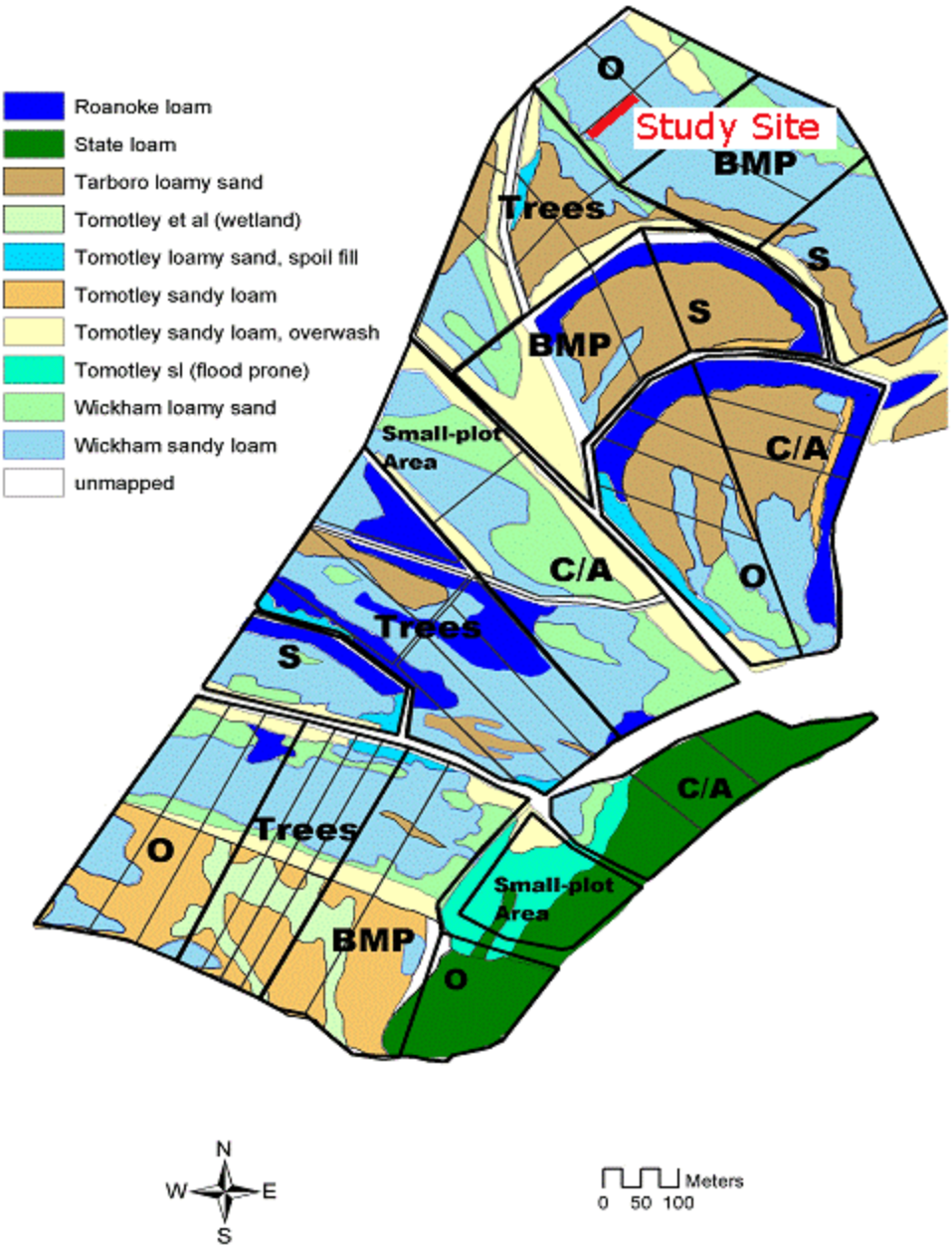

Figure 2. A map of the study site and diagnostic soils in the FSRU at CEFS in Goldsboro, NC.

Temperature, Rainfall, and Soil Moisture/Temperature - 2015 Growing Season

Hourly average precipitation and air temperature data were obtained from the NC Climate Retrieval and Observations Network of the Southeast Database (CRONOS: http://climate.ncsu.edu; Dec. 12, 2015). The actual recording instrumentation is part of the NC Environment and Climate Observing Network (NC ECONet: Latitude: 35.37935˚, Longitude: -78.0448˚, Station ID: GOLD – Cherry Research Station). The ECONet station is located approximately 0.83 km from the no-till BMP subplot monitored in this project. Soil moisture and water content within the BMP subplot were measured every 10 minutes using an EM50® Data Logger and 5TM® sensors (Decagon Devices, Inc.) inserted at a depth of 7.62 cm below the soil surface. Monthly descriptive summaries for each of these parameters are provided in Table 1 for the period April 24, 2015 to September 3, 2015.

Table 1.Total precipitation and descriptive summaries of daily air temperature recorded by NC ECONet Station GOLD-Cherry Research Station, and 10-minute readings of soil temperature and moisture content (depth: 7.62 cm) within the no-till BMP subplot monitored in this project.

Period: Date (DOY)	24 April (114)-31 May (151)	1 June (152)-30 June (181)	1 July (182)-31 July (212)	1 Aug (213)-3 Sept. (246)
	Precipitation (mm)			
Total	96.27	70.10	101.09	116.33
	Ambient Air Temperature (˚C)			
Mean	19.7	26.3	26.7	25.1
Std. Dev.	6.2	5.0	4.1	4.3
Minimum	3.4	13.6	16.7	14.2
Maximum	31.6	37.8	36.3	37.1
	Soil Moisture Content (m^3/m^{-3})			
Mean	0.162	0.078	0.074	0.115
Std. Dev.	0.027	0.020	0.034	0.039
Minimum	0.167	0.041	0.034	0.038
Maximum	0.258	0.124	0.237	0.292
	Soil Temperature (˚C)			
Mean	20.9	28.5	28.5	27.3
Std. Dev.	4.1	3.0	2.4	2.6
Minimum	14.7	21.7	23.2	21.7
Maximum	33.6	35.5	35.8	35.2

No-Till Corn

The study site subplot consists of 8 rows that are 102-m long within one rep of the no-till BMP block. A 2-row buffer was designated on either side of the subplot. Corn (*Zea mays* var. KDC 64-69, treated and Roundup® ready) was planted in the study site subplot of the BMP no-till system at a rate of 28,000 seeds ac^{-1} spaced 17.8 - 19.1 cm apart on April 24, 2015 (DOY 114). Liquid UAN was applied on April 27, 2015 (DOY 117) at a rate of 70 lbs N ac^{-1} and again on May 29, 2015 (DOY 149) at a rate of 87 lbs N ac^{-1}. Immediately after planting, pre-herbicide Bicep II Magnum (S-metolachlor + Atrazine) was applied at a rate of 2.1 qt. ac^{-1}. Immediately following sidedress N application, glysophate (Roundup) and atrazine were applied at a rate of 1 qt. ac^{-1} each.

Nitrous Oxide Measurements

Non-Steady State Vented Static Chambers – Field Measurements

The soil-atmosphere exchange of N_2O was measured at least once a week and for 3-4 consecutive days after rain events. Samples were collected midmorning of each sampling day, from April 30, 2015 (DOY 120) to September 2, 2015 (DOY 245), for a total of 30 measurement dates.

A vented, non-steady state closed-chamber technique was used (Hutchinson and Livingston, 2001). Twenty-four PVC (16 in-row, 8 between-row) anchors (20.32 cm diameter x 20.32 cm height) were inserted to a depth of 17.78 cm. The anchors were placed in 4 groups (6 anchors per group) along the length of the no-till BMP subplot (Appendix I). Anchors were installed two weeks prior to gas sampling. They were removed on May 29,

2015 (DOY 149) for the second application of UAN fertilizer. The anchors were reinserted the following day (May 30, 2015) in new positions ~ 25 cm from the original placement, and remained in place until the study completion after harvest.

For each sampling event, four anchors (one within each group) were covered with a gas-tight PVC end-cap (internal dimensions 20.32 cm in diameter x 10.15 cm in height) equipped with a septum and a vent (Hutchinson and Livingston, 2001). Each PVC end cap as purchased was equipped with a large rubber gasket. Prior to sampling, the gasket was inverted exposing the flat end of the gasket. A thin ribbon of Mortite® non-drying caulk was applied to the flat portion of the gasket. When the prepared PVC end cap was placed on the anchor, the flat portion of the rubber gasket treated with the Mortite® caulk formed an airtight seal with the flat top of the edge of the anchor. Although airtight, the seal between the PVC end cap and the anchor can be broken fairly easily and the anchor left undisturbed. Any disruption of the Mortite® caulk when removing the PVC end cap from the anchor was easily repaired in a few moments allowing the same PVC end cap to be used for repeated measurements. Accounting for the portion of the anchor above the soil interface, the total headspace when a PVC end cap was installed on an anchor was 4.115 liters.

Samples from the headspace inside the PVC end-cap anchor combination were collected using two-way needles and 100 ml evacuated glass serum vials sealed with 12.5 mm inner-diameter red rubber Suba-Seal® septa (Sigma-Aldrich Biotechnology LP) at 0, 10, 20, 30 and 40 min after the PVC end caps were seated on the anchors. The exposed glass vials were held in place for several minutes before removing the two-way needle to ensure that the internal vacuum within the glass vial had come to equilibrium with atmospheric

pressure. The evacuated glass serum vials were prepared several hours prior to sampling using a Welch™ DuoSeal™ High Vacuum pump. The rubber septa inserted into the glass vials and used to collect field samples were used only once and then discarded. Glass vial and rubber septa holding times were tested, and potential retention of N_2O by the rubber septa was also tested (Appendices C and D).

Once collected, the exposed glass vials were transported to the laboratory in Raleigh, NC, for analysis within 3 hours. Typically analysis of the collected samples was started within 4 hours after collection via manual injection using an Agilent® model 5890 gas chromatograph (Agilent Technologies) equipped with a PoraPak™ Q column (P5 carrier gas; oven temperature 60˚C), an injection valve (2 mL sample loop), and an electron capture detector maintained at 350°C. The gas chromatograph was equipped with a pre-column and used back-flushing to prevent water from entering the analytical column. Samples for manual injection were removed from each glass serum vial using a valved 5 mL polyethylene syringe. Typically samples were analyzed within 10 hours of collection. A total holding time of 24 hours was deemed acceptable using the combination of the 100 mL glass vials and the Suba-Seal® septa (see Appendix C).

A multi-point standard curve was used to derive the relationship between the gas chromatograph peak area, which is proportional to the moles of N_2O in a sample, and N_2O concentration in ppbv. A series of standard curves were generated between February 12, 2015 and September 18, 2015. Data for all the standard curves were combined and fitted using a quadratic (second-order polynomial) model via IGOR Pro® software (WaveMetrics,

Inc.). The resulting quadratic model was used to determine the concentration of N_2O in the exposed glass vials from all 30 sampling dates (Appendix B).

Individual concentrations used to derive the multi-point calibration curves were prepared using zero grade air and a NIST-traceable certified N_2O stock calibration standard (~ 50 ppmv N_2O; Airgas®) in combination with a Teledyne® model T700 gas dilutor (Teledyne Advanced Pollution Instrumentation). The outlet from the Teledyne model T700 unit was connected to a Nylon manifold equipped with a septum for sampling. Output from the manifold was connected to 30.5 m of reinforced PVC tubing to prevent contamination of the standards by backflow of ambient air into the manifold during collection. The dilutor was operated for approximately 10 minutes at each selected concentration to ensure that the manifold-tubing combination was at equilibrium with the desired N_2O concentration. The use of the manifold allowed aliquots of the desired standard N_2O concentration to be obtained using either syringes equipped with valves or evacuated glass serum bottles. These in turn were immediately injected into the gas chromatograph following collection.

Non-Steady Vented State Static Chamber - Flux Calculations

The approach of Pedersen et al. (2010) was adopted to calculate flux from the non-steady state static chambers. The approach is built on the assumption that temporal measurements of the concentration of N_2O in the headspace of non-steady state static chambers is inherently non-linear, even though such plots may often appear to be linear when N_2O concentration is plotted versus time. The approach of Pedersen et al. (2010) is based on a specific application of the non-linear model proposed by Hutchison and Mosier (1981), deemed the HM model. The approach developed by Pedersen et al. has been coded into a

package for operation via R statistical software (http://www.r-project.org) and is readily available to all potential users. The developed model is referred to as the HMR package. Use of the HMR package to calculate flux derived from non-steady state static chambers has been recommended when the available number of data points per chamber is ≥ 4, and ancillary soil data is not sufficient to allow use of more complicated fitting routines (de Klein and Harvey, 2015).

The HMR package does not directly solve for flux, but includes estimates of flux at time zero as one of two fitting parameters to minimize the mean standard error. The HMR package provides several options for manual or automated execution. For this project, the manual mode was selected, allowing individual review of each set of chamber data. The HMR package makes recommendations as to whether the data adhere to the requirements for a solution via the HMR model, or should be fit with a simple linear regression. Output from the execution of the HMR package is provided in the standard csv text file format. In this project, with the input parameters selected (anchor area, sampling time in minutes, headspace volume of PVC end cap plus anchor, N_2O concentration as ppmv), the flux estimates obtained using the HMR package had units of μL of N_2O m^{-2} min^{-1}. These units were subsequently converted to mg N_2O per m^{-2} $hour^{-1}$ using the ideal gas law and the recorded ambient air temperature at the time of sampling.

For the 120 non-steady state static chamber measurements, the HMR package recommended 55% be processed using the HMR model. The remaining 45% were processed using a linear regression, calculating flux from the slope of the linear model. The 55% of the non-steady state static chamber measurements processed with the HMR model were also

separately processed using linear regression to provide a measure of the under prediction if only linear regression had been used to estimate flux. On average, the linear regression approach compared to the HMR model yielded an underestimate of ~24%, with a range of 1 to 151%. When the estimated actual flux values derived using linear regression are plotted versus those derived from the HMR package, the relationship is linear up to ~ 2500 µg N_2O m^{-2} $hour^{-1}$ (Figure 3), which is consistent with the results of Pedersen et al. (2010).

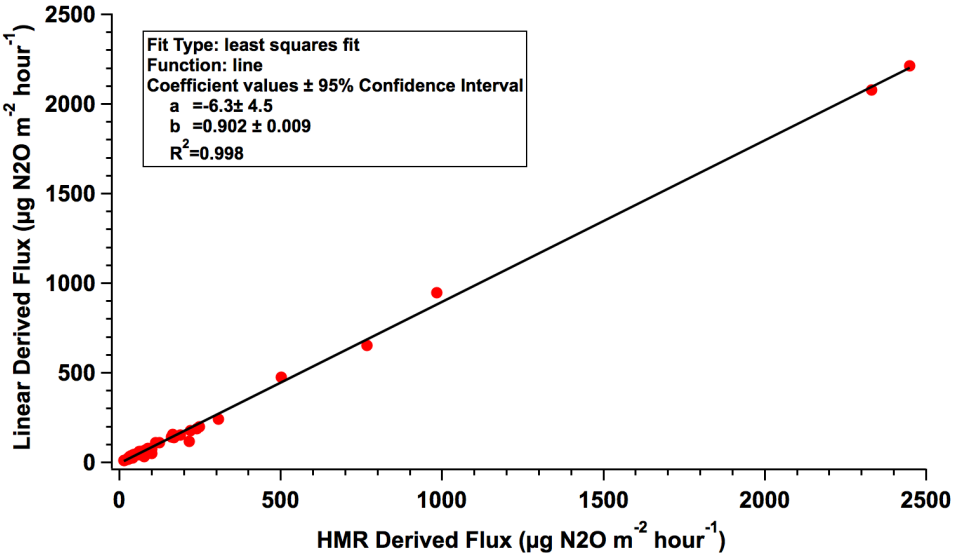

Figure 3. Estimated N_2O flux derived using linear regression versus the HMR model for 55% of the observations obtained using the non-steady state static chambers.

To create the final data set of N_2O flux values obtained using the non-steady state static chambers for use in this project, the flux values derived using the HMR package were combined with the remaining values derived using linear regression (Appendix A). As indicated by the slope (b-value) in Figure 3, the N_2O flux values obtained using linear regression may be biased low by ~ 10%.

Simple Flow-Through Chambers – Field Measurements

A simple flow-through chamber design was used to provide an index of the temporal pattern in N_2O emissions from May 5, 2015 (DOY 125) to September 2, 2015 (DOY 245). A total of 4 positions were sampled (one per group of 6 PVC anchors) along the length of the no-till BMP subplot (Appendix I). The simple flow-through chambers were rotated among the 6 anchors within a group and were repositioned following a rain event. The chamber was left in place on a given anchor until the next significant rain event. The chambers were moved within ~ 1.5 weeks if no significant rainfall events occurred in that period of time. Due to the expense and time required to calibrate the flow-through system, the simple flow-through chambers were not used to estimate N_2O flux. Instead the data gathered using the flow-through chambers were used to inform further refinements in calculating cumulative N_2O flux across the 4 groupings of PVC anchors within the no-till BMP subplot.

Design of the simple flow-through chambers was based on the PVC end caps used for the non-steady state static chambers. Instead of the septum and single vent port, the top of PVC end caps were fitted with three John Guest® straight bulk-head unions (3/8" OD, ¼" ID; Cole-Parmer, Vernon Hills, IL). Two of the bulk-head unions were used as static ports to allow air to pass into or out of the chamber. Each was fitted with a 25 cm vertical length of Teflon® rigid-wall tubing. The third bulk-head union was connected by Nylon reinforced PVC tubing to a gas sampling system used to systematically sample the N_2O concentration in the head space formed by the PVC end cap and corresponding anchor.

The gas sampling system consisted of a series of solenoid valves, common manifolds, and pumps that controlled air flow to and from each simple flow-through chamber. Each

chamber was connected to one-side of a compact directional control 3-port brass solenoid valve (McMaster-Carr, Atlanta, GA). The remaining 2 ports on an individual solenoid were connected either to a common manifold or to the primary gas-sampling manifold. In the default (OFF) position, the solenoid allowed airflow from the common manifold and separate pump (Thomas® Compressor/Vacuum pump 1/8 hp; Grainger™) to flow towards and into the simple flow-through chamber. Continuously flushing the gas sampling line from each chamber prevented condensation of water and also provided air movement through the chamber when not being sampled. The air pumped into the simple flow-through chambers exited through the two static ports in the PVC end-cap. When a solenoid was switched to the ON position, airflow from a single simple flow-through chamber was pulled toward the instrument shelter and into the gas-sampling manifold. This was achieved by use of a second pump of similar design.

With this configuration, the two pumps operated continuously ensuring that there was always airflow through all sampling lines and chambers. Rate of airflow to or from a simple flow-through chamber was controlled using acetal push-to-connect critical orifices (McMaster-Carr, Atlanta, GA) mounted in the respective manifolds. In this study, the common manifold allowed airflow of ~ 3.8 LPM from the instrument shelter towards an individual simple flow-through chamber. The gas-sampling manifold was equipped with a series of critical orifices of varying size allowing the gas-sampling rate to be easily changed by selecting a different critical orifice mounted on the manifold. For most of this study, the gas sampling flow rate from an individual chamber was set at 2.8 LPM. A variety of John Guest® fittings were used with the gas sampling lines, solenoids, pumps and manifolds to

allow rapid and leak-proof connections when assembling, repairing or changing the configuration of the gas sampling system.

Control of the sampling sequence of the solenoids and their respective simple flow-through chambers was achieved using an ARDUINO® microprocessor (Adafruit™: http://www.adafruit.com/arduino; Dec. 12, 2015) programmed to change sampling positions every 30 minutes (Appendix H). Output from the microprocessor was used to toggle a separate DC/AC solid-state switch, which turned a solenoid to the ON or OFF position. A separate DC voltage output from the microprocessor was used to monitor which solenoid was currently in the ON (sampling) position. A fifth solenoid was used to sample ambient air at a location mid-way along the BMP sub-plot at approximately 45 cm above the soil surface.

Once initiated the microprocessor operated independently, sequentially stepping through each of the 5 sampling positions – 4 simple flow-through chambers and ambient atmosphere. The sampling sequence could be easily restarted by simply powering off, then powering on the ARDUINO microprocessor. For this study, each sampling position was monitored for 30 minutes, 9 times a day (2.5 hour sampling interval). A set of readings from each of the 4 simple flow-through chambers was bracketed by an ambient N_2O concentration reading, which proved useful in monitoring and correcting for drift in the gas analyzer.

A Teledyne® model 320EU nitrous oxide analyzer (Teledyne Advanced Pollution Instrumentation) was used to determine the concentration of N_2O in the gas sampling stream from each sampling position. The gas analyzer was checked weekly or bi-weekly using Tedlar® bags (DuPont) containing either zero air or 2000 ppbv N_2O. The Teledyne model T700 gas dilutor referenced above was used to generate zero air or known concentrations of

N_2O and to fill the Tedlar bags. Each Tedlar bag was fitted with a quick disconnect adaptor allowing direct connection to the inlet of the Teledyne model 320EU instrument.

Raw output from the Teledyne model 320EU instrument, as well as the position voltage output from the ARDUINO microprocessor corresponding to the operational state of a given solenoid, was recorded using DAQPlot® (VVimaging, Inc.) software operating on a MacBook Pro® laptop running Ver. 10.9 of the Macintosh™ operating system. The software provided a real-time visual display of trends in N_2O gas concentrations being recorded for a given sampling position, as well as the capacity to look at trends in gas concentrations across periods of several days. The data recorded by the DAQPlot software was downloaded to a common text file format weekly, or more frequently as deemed necessary.

Simple Flow-Through Chambers – Data Processing

The raw output from the Teledyne model 320EU gas analyzer required further processing to obtain the desired temporal curve of N_2O emissions. The exported text file from the DAQPlot software was first imported into an EXCEL® spreadsheet and reviewed for any inconsistencies. Periods when the instrument was calibrated using zero air and the known concentrations of N_2O were removed from the dataset, and the position voltage output from the ADRUINO microprocessor was normalized with a unique identifier for each voltage corresponding to a sampling position. A csv formatted text file was then generated from the EXCEL spreadsheet and used for input to a custom Python® computer code (Ver. 3.5), which calculated the average N_2O concentration in the headspace of the simple flow-through chamber during the last 4 minutes of a 30-minute sampling period. This calculated average N_2O concentration, along with position identifier, and date and time at the end of the

respective 30 minute sampling time were output and used to make subsequent temporal plots of N_2O concentration within a given simple flow-through chamber for each sample position, including ambient air. Net N_2O concentration was calculated for the headspace of the simple flow-through chambers by subtraction of the average ambient N_2O concentrations recorded at the beginning and end of each set of 4 readings from the chambers at each respective group location.

Simple Flow-Through Chambers – Instrument Shelter

All instrumentation, computers, and pumps required for operation of the simple flow through chambers were housed in an air-conditioned trailer located adjacent to the no-till BMP subplot. An industrial generator supplied AC power to operate the instrumentation. The generator operated continuously except for required maintenance every 250+ hours. Typically the required maintenance lasted only 10 minutes, and then the generator was restarted. Several uninterruptable power supplies were able to keep all instrumentation, and computers operational during these 10-minute maintenance periods. The pumps and the air conditioning unit were turned off, however, resulting in no data collection. Overall, ~2 days of data were lost when the generator ran out of fuel, and ~ 5 days of data near the end of the monitoring period were lost due to a computer malfunction.

Statistics

Descriptive statistics for various datasets were calculated using the EXCEL® spreadsheet computer software from the Microsoft Corporation.

Results

For the period April 24 to September 3, 2015 (DOY 114 – 246), the no-till BMP subplot received 378.7 mm of rainfall (Figure 4). According to the National Oceanic and Atmospheric Administration (NOAA) National Center for Environmental Information (*https://www.ncdc.noaa.gov/cdo-web/datatools/normals*), average rainfall for a comparable period is ~ 484 mm for Goldsboro, NC. In comparison with the multi-year averages, the 2015 growing season was relatively dry with a deficit of ~ 100 mm of rainfall (~ 4 inches) that resulted in periods of moisture stress for the corn crop. Almost a third of the precipitation received in 2015 occurred within the first 17 days of planting (DOY 114 – 131) and within 14 days of the first application of N fertilizer (DOY 117). The bulk of this input (61 mm) arose from the passage of tropical storm Ana on May 9 – 11th (DOY 129 – 131). The antecedent soil moisture was already relatively high due to rainfall events prior to DOY 114 (data not shown). The additional intense rains from tropical storm Ana resulted in near saturated conditions, with standing water being observed within portions of the subplot at least 24 hours after passage of the storm.

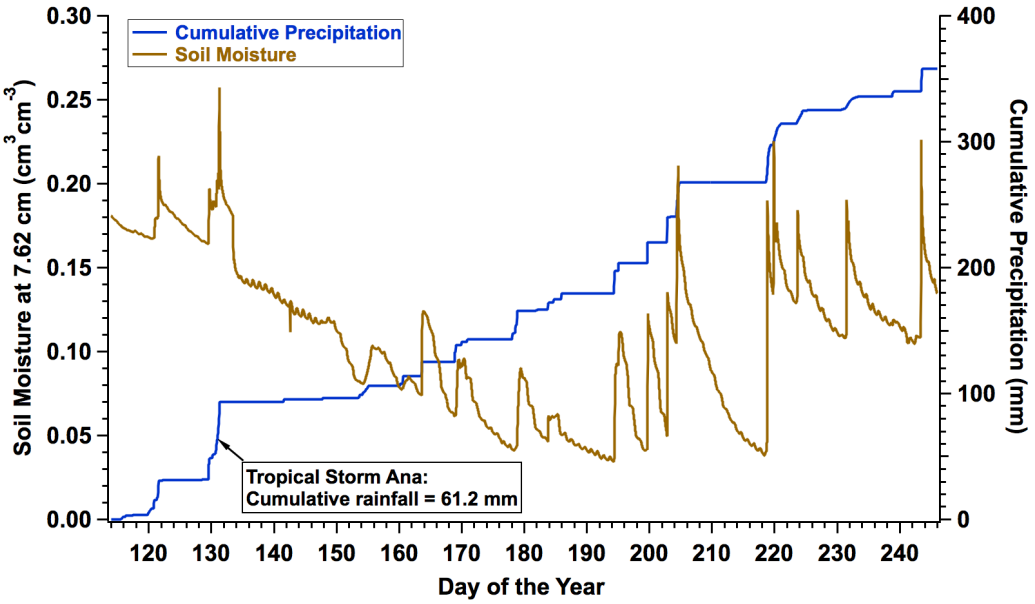

Figure 4. Soil moisture content at 7.62 cm depth and cumulative rainfall for the period April 24, 2015 (DOY 114) to September 3, 2015 (DOY 246).

Following passage of tropical storm Ana, soil moisture continued a steady decline until about July 13, 2015 (DOY 194) (Figure 4). During this same period, ambient air temperatures and soil temperatures increased, reaching some of the highest temperatures recorded during the growing season (Figure 5). From DOY 160 to 220 (June 9th – August 8th, 2015), soil temperatures were at or above 25˚C, with daily peak values reaching 35˚C or higher in the upper surface of the soil. Recovery of soil moisture began after DOY 194 (July 13, 2015) with increasing frequency of rainfall, but again declined between DOY 210 – 220 (July 29th – August 8th, 2015). After August 8, 2015, ambient air temperatures lowered as did soil temperatures, as the frequency of rainfall events increased. However, soil moisture levels did not recover to the extent of those observed at the start of the growing season. Approximate monthly totals and descriptive summaries for ambient air temperature, soil temperature and soil moisture content are given in Table 1.

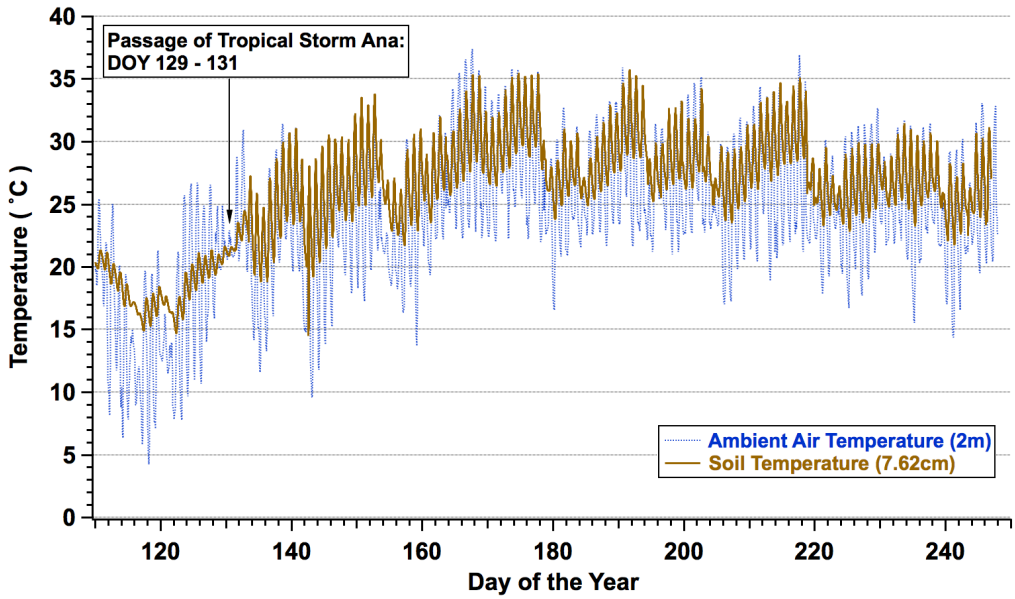

Figure 5. Ambient air temperature (2m) and soil temperature at 7.62 cm depth for the period April 24, 2015 (DOY 114) to September 3, 2015 (DOY 246).

Observations of N_2O flux derived from the individual non-steady state static chambers within the groups along the length of the no-till BMP subplot are plotted as a function of time in Figure 6. Highest flux was observed immediately after the passage of tropical storm Ana. As noted in Figure 6, these high fluxes correspond to relatively high soil moisture content as a result of both the antecedent soil moisture levels before the storm and the additional ~ 61 mm of rainfall over the course of a 48-hour period. The high fluxes are also linked to the initial application of N fertilizer on DOY 117. Closer inspection of Figure 6 reveals that this period of relatively high N_2O flux was short lived, and the absolute magnitude of the flux was highly variable within the 4 groups of anchors along the length of the subplot. A descriptive summary of the N_2O values derived from the non-steady state static chambers as a function of group (position along the subplot) is provided in **Table 2**.

The highest individual N_2O flux values measured with the non-steady state static chambers were at groups 1 and 2 (18.72 and 5.69 mg N_2O m^{-2} h^{-1}, respectively). The individual mean values within a group also reflect the variation in N_2O emissions across the subplot. However, the median values are actually very similar in magnitude suggesting that the bulk of the observations of N_2O emissions during the 2015 season were similar. This is also evident in comparing the 75% quartiles for each group (**Table 2**). This agreement in the majority of N_2O flux measurements along the length of the subplot is probably due in part to the relatively dry conditions and elevated soil temperatures observed after passage of tropical storm Ana. Highest variations in N_2O flux appeared to be related with soil moisture content, and therefore indirectly rainfall frequency. This trend is apparent when the percent relative standard deviation among 4 chambers sampled on a given date is plotted as a function of DOY (Figure 7). Early in the season, percent relative standard deviation among the 4 chambers within a single day's measurement could exceed 150%. Under the driest conditions (e.g. DOY 180 – 195), the relative standard deviation was < 20%. Upon arrival of more frequent rainfall in late summer and early fall, the percent relative standard deviation associated with measurements among 4 chambers in a single day ranged from 30 – 80% (Figure 7). However, it is important to note that regardless of the soil moisture status within the subplot, quantifiable amounts of N_2O emissions were detected on all sampling dates using the non-steady state static chambers.

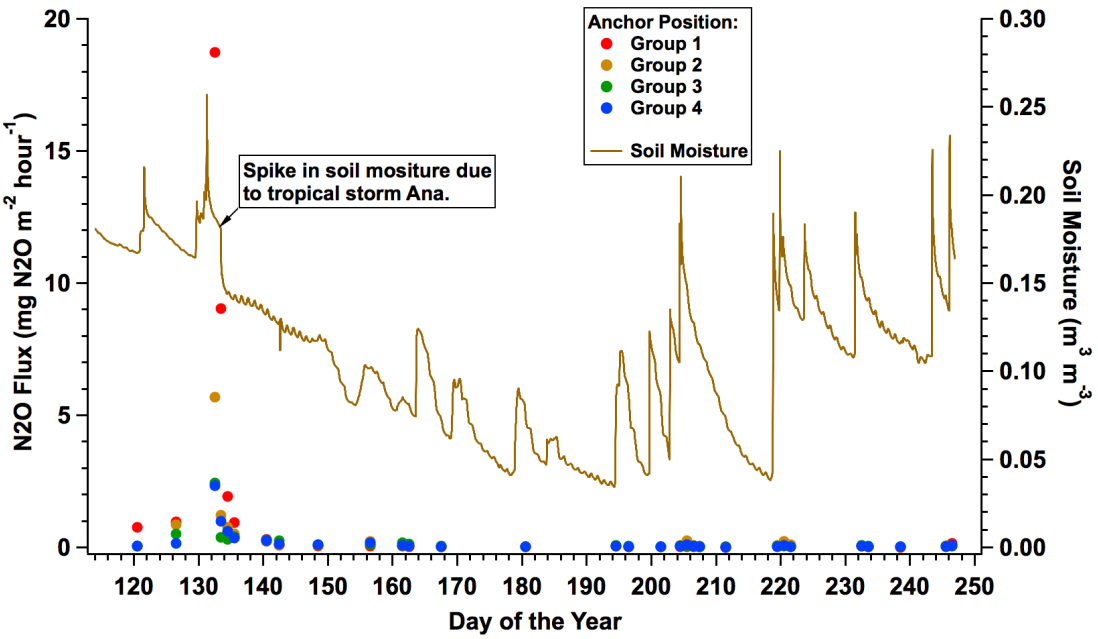

Figure 6. Nitrous oxide flux measured using non-steady state static chambers as a function of group position and soil moisture content as a function of Day of the Year for the period April 24, 2015 (DOY 114) to September 3, 2015 (DOY 246).

Table 2. Descriptive summary of N_2O flux as measured by the non-steady state static chambers as a function of group for the period April 24, 2015 (DOY 114) to September 3, 2015 (DOY 246).

	Non-Steady State Static Chamber Flux (mg N_2O m^{-2} h^{-1})			
Chamber Group:	**1**	**2**	**3**	**4**
Mean	1.123	0.367	0.199	0.200
Median	0.042	0.062	0.059	0.051
Std. Dev.	3.717	1.046	0.445	0.451
Minimum	0.010	0.013	0.013	0.011
Maximum	18.720	5.691	2.449	2.332
25th percentile	0.031	0.042	0.041	0.031
75th percentile	0.148	0.219	0.173	0.129

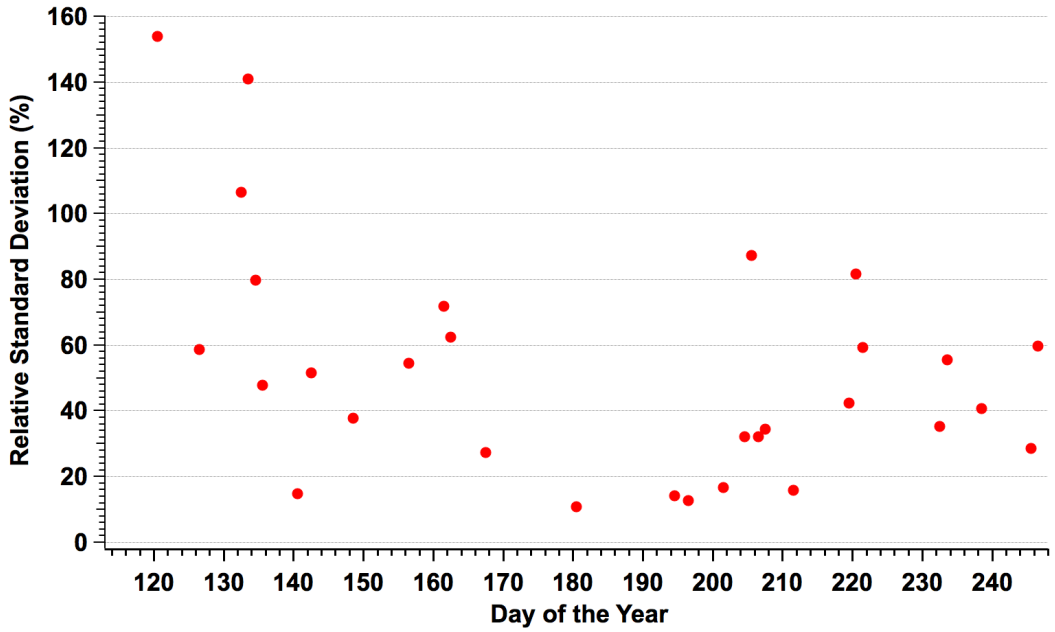

Figure 7. Percent relative standard deviation of individual sets (n=4 chambers per set) of N_2O flux measurements using the non-steady state static chambers as a function of Day of the Year for the period April 24, 2015 (DOY 114) to September 3, 2015 (DOY 246).

An example of the temporal data on N_2O emissions obtained using the simple flow-through chambers is illustrated in Figure 8 for the PVC anchors located in the group 1 position for the period May 5, 2015 (DOY 125) to September 2, 2015 (DOY 245). As with the non-steady state static chambers, the maximum average net N_2O concentrations recorded in the headspace of the simple flow-through chambers coincided with the spike in soil moisture content associated with the passage of tropical storm Ana. The net concentration of N_2O in the headspace diminished coincident with the N_2O fluxes calculated using the non-steady state static chambers (Figure 8). No further peaks in net N_2O concentration were observed for the remainder of the observation period, and further discussion of the simple flow-through chamber data will focus only on the peak in emissions associated with the passage of tropical storm Ana.

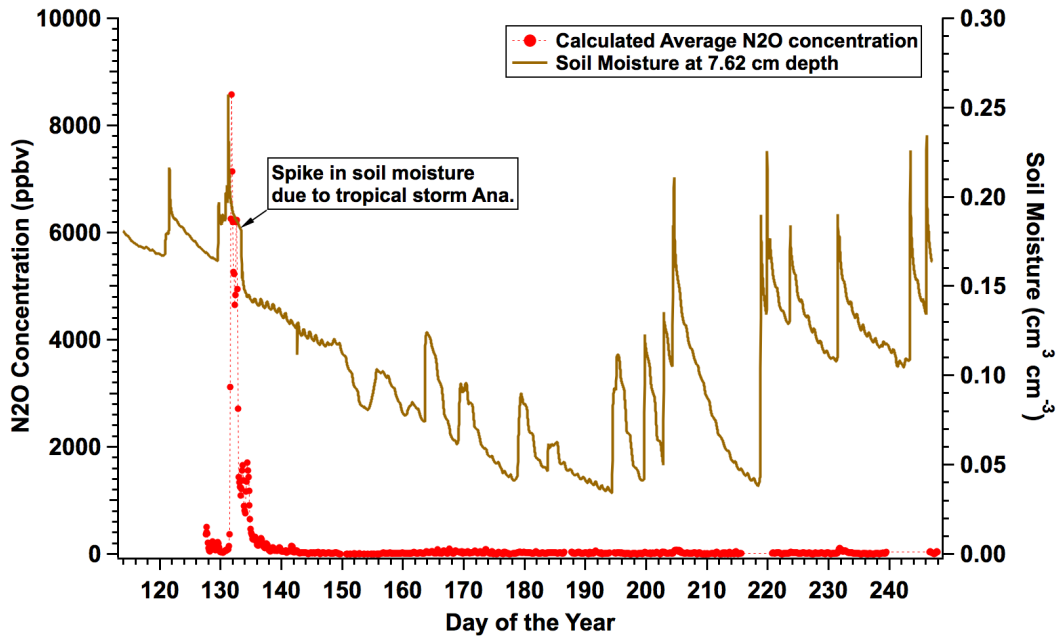

Figure 8. Net concentration of N_2O in headspace of simple flow-through chambers (group 1 position) and soil moisture content at 7.62 cm depth for period May 5, 2015 (DOY 125) to September 2, 2015 (DOY 245). Dashed line added to aid visual identification of trend between individual data points for N_2O concentration.

A comparison between the net average N_2O concentrations calculated for the headspace for all 4 simple flow-through chambers at the group 1 – 4 positions is shown in Figure 9. Also graphed are the individual hourly precipitation amounts that were recorded by the nearby ECONet station during the passage of the storm. The net average N_2O concentrations in the headspace of the chambers mirrors the trends in N_2O flux calculated from the non-steady state static chambers. Highest net N_2O concentrations were recorded for the group 1 and 2 positions, while substantially lower net N_2O concentrations were associated with chambers at the group 3 and 4 positions (Figure 9). This simple visual comparison suggests that the net N_2O concentrations obtained using the simple flow-through chamber design do serve as an index in the strength of N_2O flux, and that the temporal

pattern demonstrated in Figure 8 does mirror to some degree the change in N_2O emissions over time and space within the no-till BMP subplot.

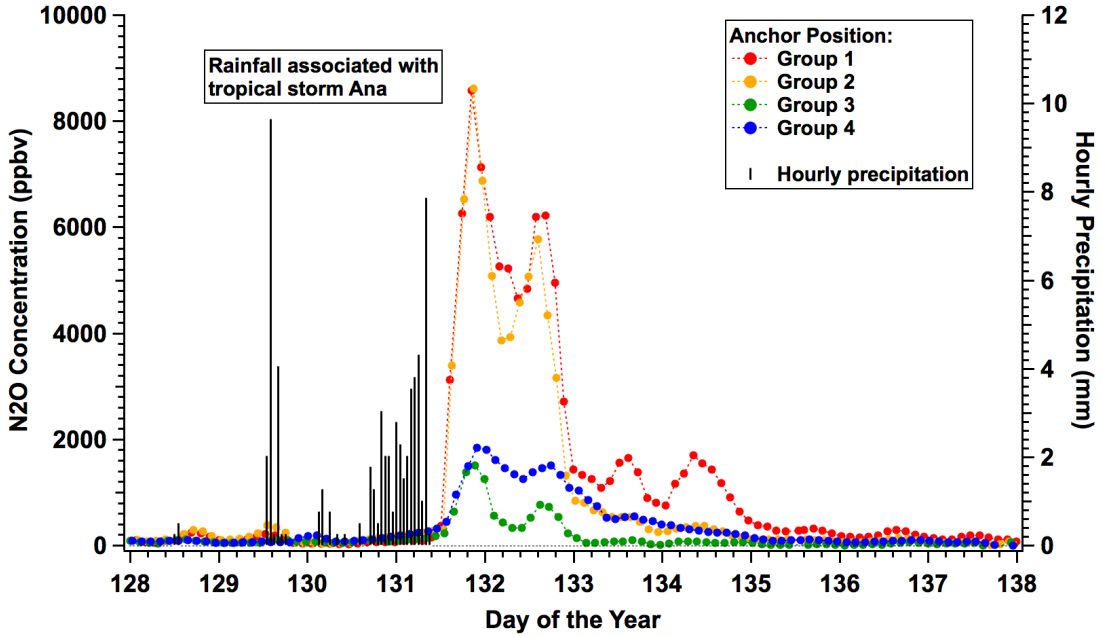

Figure 9. Net concentration of N_2O in headspace of simple flow-through chambers (groups 1 - 4) and hourly precipitation amounts for the period May 8, 2015 (DOY 128) to May 18, 2015 (DOY 138). Dashed line added to aid visual identification of trend between individual data points for N_2O concentration.

From Figure 9, it appears the peak in N_2O emissions may have occurred at ~ midnight on May 12, 2015 (DOY 132) and ended 4 days later on May 16, 2015 (DOY 136). To explore further the relationship between the end of measureable rainfall and the peak in N_2O emissions, the x-axis in Figure 10 was expanded to focus only on the period May 11, 2015 (DOY 131) to May 15, 2015 (DOY 135).

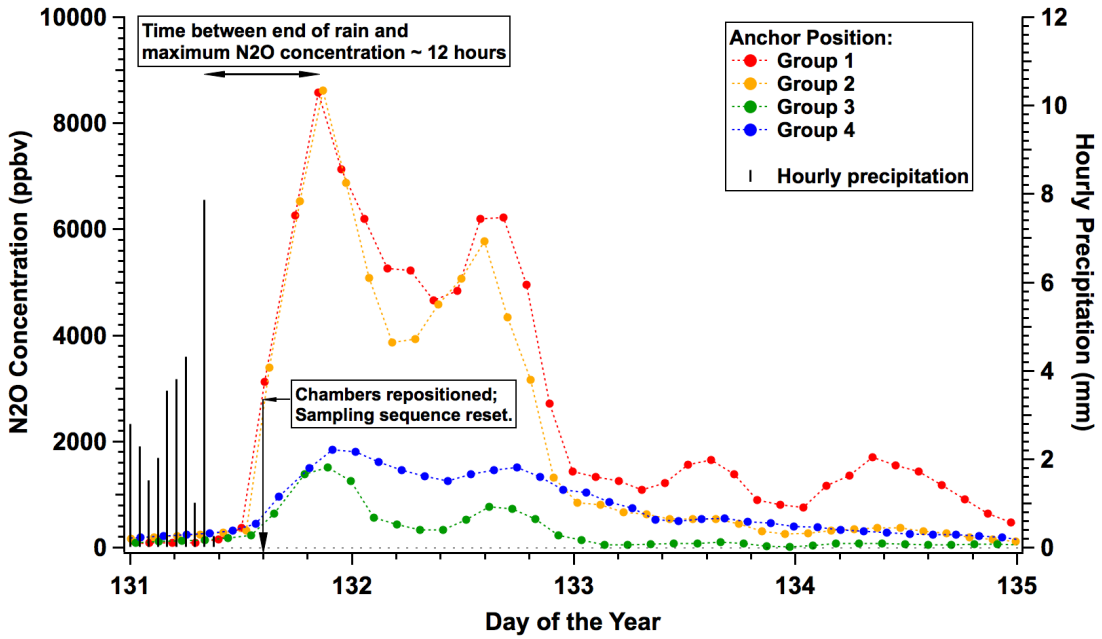

Figure 10. Net concentration of N_2O in headspace of simple flow-through chambers (groups 1 - 4) and hourly precipitation amounts for the period May 11, 2015 (DOY 131) to May 15, 2015 (DOY 135). Dashed line added to aid visual identification of trend between individual data points for N_2O concentration.

The last measureable rain recorded on May 11, 2015 (DOY 131) ended at approximately 8:00 hours in the morning. By mid-afternoon, the simple flow-through chambers had been moved according to protocol and the sampling sequence reset at ~ 15:00 hours (Figure 10). The trend in the individual data points for the net average N_2O concentration for each group in Figure 10, after repositioning of the simple flow-through chambers, suggests that the flux in N_2O was still continuing to increase and had not reached a maximum. Each sampling position, including ambient air, was sampled every 2.5 hours, thus the separation between individual data points within the same group (color) represents ~2.5 hours. Based on the change in the net average N_2O concentrations in Figure 10, the peak in N_2O emissions occurred ~12 hours after the end of the last measureable rainfall. Furthermore, the peak in N_2O emissions seemed to be consistent at all sampling locations

within the no-till BMP subplot, even though the relative strength in N_2O emissions varied substantially as indicated by the non-steady state static chamber measurements. This observation, at least in this one set of data, indicates that the differences in the observed magnitude of the N_2O flux measured by the non-steady state static chambers (Figure 6), and suggested by the simple flow-through chambers (Figure 10), are dependent primarily on local conditions within the no-till BMP plot, and do not arise because of differences in the time of peak emissions of N_2O between the group positions. In other words, comparisons of the magnitude of N_2O flux between the 4 group sampling positions within the subplot (**Table 2**) are valid, since all 4 group positions appear to reflect the same temporal pattern in N_2O emissions.

Discussion

Cumulative N_2O Emissions for 2015 Growing Season

The combination of the results from the non-steady state static chambers and the simple flow-through chambers allowed three ways to calculate the cumulative N_2O flux for the period April 24 to September 3, 2015 (DOY 114 – 246) from the no-till BMP subplot. The first approach (LII) only uses the data from the non-steady state static chambers (Appendix A). Cumulative flux is derived as the linear interpolation between individual N_2O flux measurements on individual dates and the integration of the area under the resulting curve. For the majority of observations in 2015, this approach is satisfactory as the flux values are low and relatively constant across the growing season (Figure 6). However, this approach is not satisfactory to describe the peak in N_2O emissions immediately following the

passage of tropical storm Ana (DOY 131 – 136), and can lead to bias in the estimate of the cumulative N_2O flux. This is illustrated in Figure 11.

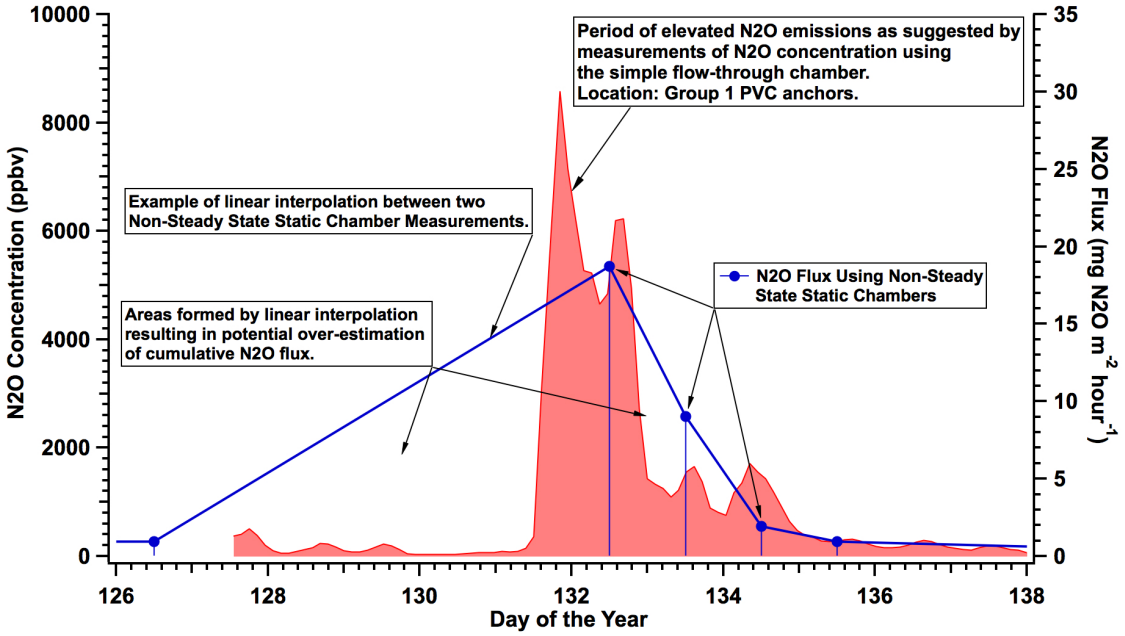

Figure 11. Illustration of linear interpolation between individual non-steady state static chamber measurements. Period of elevated N_2O emissions as suggested by measurements of N_2O concentrations using the simple flow-through chambers added to facilitate visual interpretation of data. Period: May 6 (DOY 126) to May 18 (DOY 138), 2015.

Since the time of the start in peak N_2O emissions is generally not known using the non-steady state static chamber technique, interpolating between measurements with the static chambers prior to and just after a rain event can lead to an over-estimate of N_2O flux. This positive bias varies with the intensity of the N_2O emissions following a rain event. As suggested in Figure 11, and comparing the trend in N_2O concentrations among the 4 groups using the simple flow-through chambers in Figure 10, the time of the last non-steady state chamber measurement before the event, the time after the start of the event of the non-steady state chamber measurement, and the relative intensity of N_2O emissions across the sampling positions, all interact to increase the uncertainty in the estimated cumulative flux. As a result,

at least for the data obtained in 2015 from the no-till BMP subplot, the flux of N_2O derived solely from the non-steady state static chambers is probably biased high, with a large amount of uncertainty.

The second method (LIIS), offering a possible improvement to the LII approach, uses the results from the simple flow-through chambers to estimate the start of the increase in N_2O emissions induced by the passage of tropical storm Ana. As noted above, all 4 group positions within the subplot appear to experience the start of the increase in N_2O emissions at approximately the same time (Figure 10). In this study, the start of the N_2O event induced by the rainfall associated with tropical storm Ana was assigned as 12:00 hours on May 11, 2015 (DOY 131.5; Figure 12).

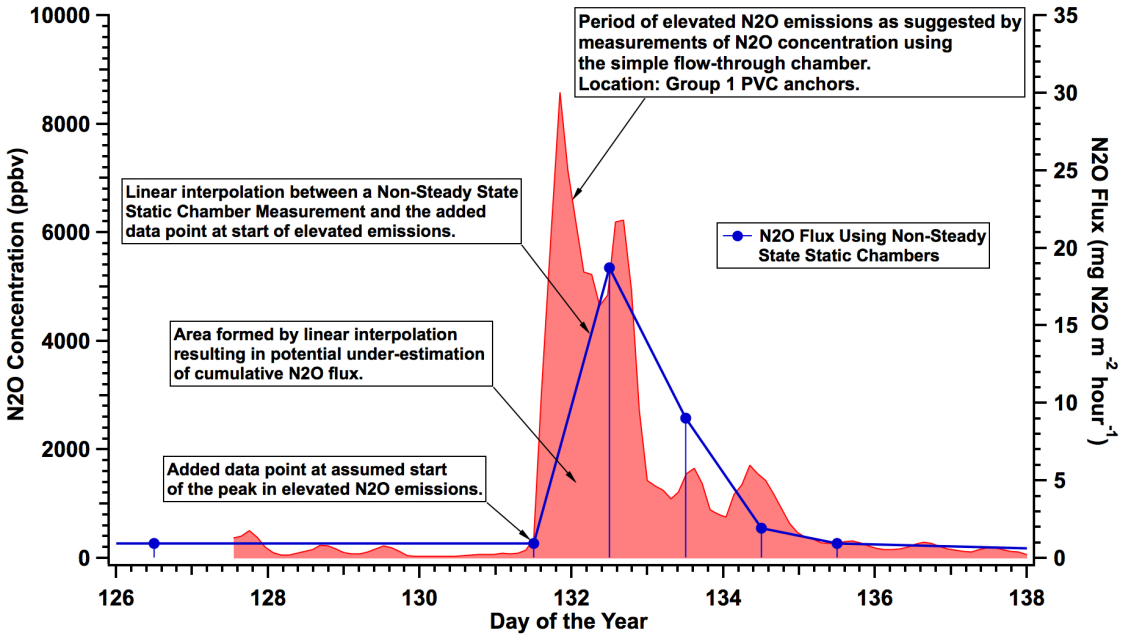

Figure 12. Illustration of linear interpolation between individual non-steady state static chamber measurements with an added data point reflecting an estimate of the start of elevated N_2O emissions (DOY 135.5). Period of elevated N_2O emissions as suggested by measurements of N_2O concentrations using the simple flow-through chambers added to facilitate visual interpretation of data. Period: May 6 (DOY 126) to May 18 (DOY 138), 2015.

The N_2O flux, as measured by the non-steady state static chamber prior to the start of the event, was then assumed to have remained constant up to DOY 131.5. Linear interpolation was then carried out between the measurements from the non-steady state static chambers accordingly (Figure 12). Including an estimate of the start of the increase in N_2O emissions decreases the potential to over-estimate the cumulative flux when interpolating from the previous non-steady state static chamber measurement, but probably leads to an under-estimation of the cumulative flux, depending upon the intensity in N_2O emissions, the rate of decline in N_2O emissions and the time of the next non-steady state static chamber measurement following the start of the increase in N_2O emissions (Figure 12). For this study, given the variation in intensity in N_2O emissions across the no-till BMP subplot, as revealed among the 4 groups of PVC anchors (Figure 10), simply correcting for the start of the increase in N_2O emissions induced by rainfall from tropical storm Ana probably results in lower cumulative N_2O emissions with perhaps reduced uncertainty.

The third approach for calculating cumulative N_2O flux for the 2015 growing season (LIISD) was to combine all data from the two different measurement techniques. In order to accomplish this, the relative measure of N_2O emissions, obtained from the simple flow-through chambers, was linked to actual N_2O flux measurements, since the data from the simple flow-through chambers was expressed only as the concentration of N_2O in the headspace of the chambers. The only measurements of N_2O flux were from the non-steady state static chambers.

As already noted, the simple flow-through chambers provided a measure of the start of the increase in N_2O emissions following the passage of tropical storm Ana (Figure 8). The

simple flow-through chambers also provided an index for the time of peak N_2O emissions observed among the 4 group positions along the subplot as well as an index of the rate of decline in N_2O emissions (Figure 10). With this additional information, it was concluded that the decrease in peak N_2O emissions at each position sampled along the subplot could best be described using a simple exponential decay curve:

$$\text{static chamber } N_2O \text{ flux} = Ae^{(-Bx)} \quad (2)$$

where x is time since the peak flux in hours, B is the decay constant, and A is the peak in N_2O flux. An estimate of the decay constant (B) was obtained by plotting the linear form of Eq. 2 as the natural log of N_2O concentration measured with the simple flow-through chambers as a function of time relative to the observed peak in N_2O concentration (time equals zero hours) and fitting a linear regression through the data. The estimate of the decay constant (B) was obtained from the slope of the fitted line (Figure 13).

Using the results from the 4 simple flow-through chambers four estimates of the value of B, the decay constant, were obtained. The estimates were essentially similar in magnitude ranging from 0.0341 to 0.0440. For the purposes of this study, the four estimates were combined to derive an average estimate of B of 0.0384 (± 0.0047; RSD = 12.3%). Since the decline in N_2O emissions among the 4 simple flow-through chambers occurred approximately across the same time period (Figure 10), it was assumed the declines in N_2O emissions were influenced by the same factors at each sampling position along the no-till BMP subplot.

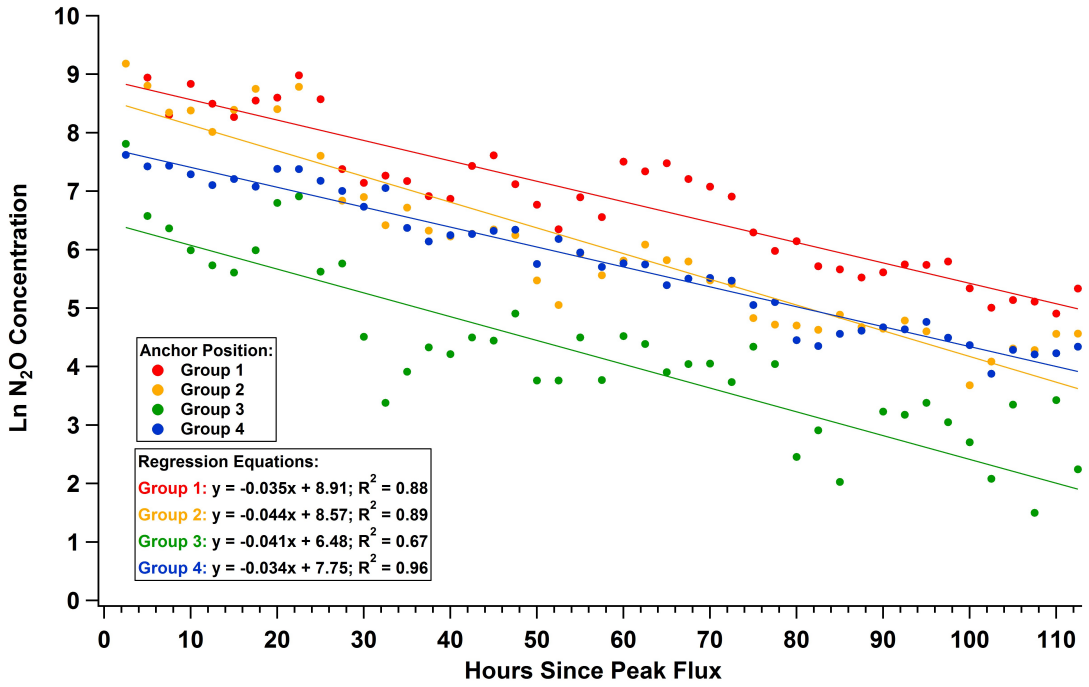

Figure 13. The natural log of the N_2O concentration from the simple flow-through chambers versus time since the peak N_2O concentration and a function of group sampling position. Period: DOY 131.849 to DOY 136.432.

Values of A, the peak in N_2O flux, for each sampling position along the no-till BMP subplot were obtained by solving Eq. 2 for A using the flux values derived from the non-steady state static chambers, accounting for the time of the static chamber measurements relative to the observed peak in N_2O concentrations. With this approach, Eq. 2 is essentially calibrated relative to the flux values derived from the static chamber technique. In other words, the relative measure of N_2O emissions obtained from the simple flow-through chambers is linked through Eq. 2 to actual N_2O flux measurements derived from the non-steady state static chambers. An example of the calculated N_2O flux using Eq. 2 as compared to the non-steady state static flux chamber measurements for the peak in N_2O emissions following tropical storm Ana is shown in Figure 14. Using the approach outlined above, the

calculated peak N_2O fluxes values (A terms) were 38.3, 11.6, 5.0 and 4.8 mg N_2O m^{-2} h^{-1} for group positions 1, 2, 3 and 4, respectively.

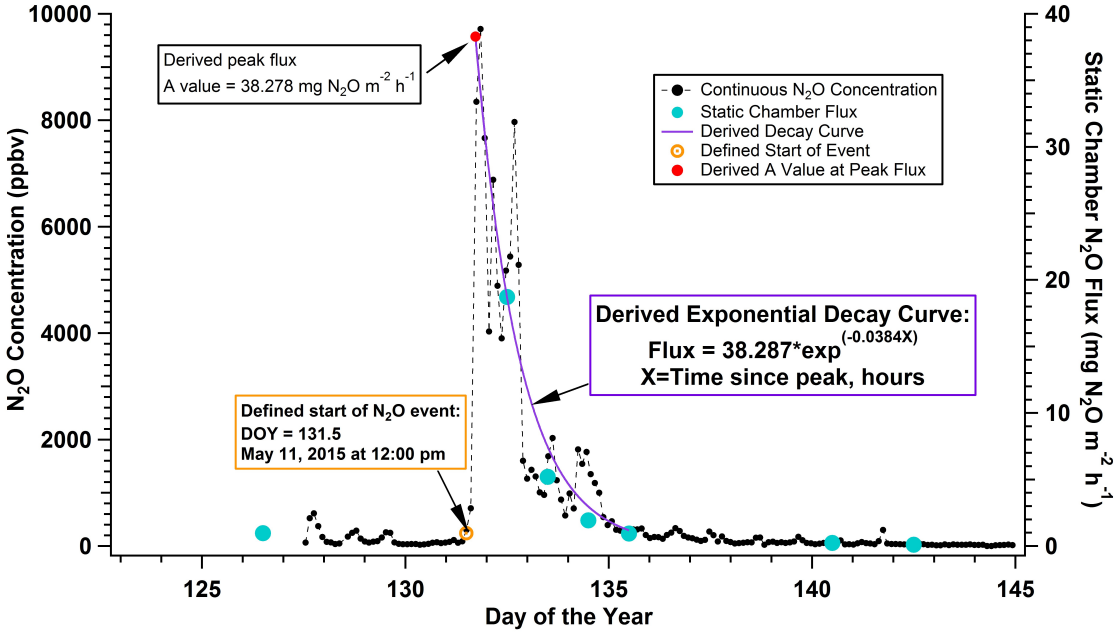

Figure 14. Comparison between estimated N_2O flux using an exponential decay function versus individual measurements of N_2O flux derived from non-steady state static chamber measurements for the group 1 sampling position. Period: DOY 131.5 to 140.5.

With Eq. 2 solved for each sampling position along the no-till BMP subplot, cumulative N_2O flux was obtained by linear interpolation up to the defined start of the peak in N_2O emissions (DOY 131.5), plus the area under the curve defined by Eq. 2 for each sampling position from DOY 131.724 to DOY 135.494, and then again by linear interpolation between non-steady state static chamber measurements from DOY 135.5 to the end of the study. There was also an inherent maximum uncertainty in the estimated peak in N_2O emissions due to the maximum sampling interval of 2.5 hours.

The cumulative N_2O flux values derived using the three approaches described above for the period April 30 to September 3, 2015 for the no-till BMP subplot are shown in Figure

15. The highest cumulative N_2O flux estimate (1009 ± 827 mg N_2O m^{-2}) was obtained from just the non-steady state static flux chamber data in combination with linear interpolation between sampling dates (LII).

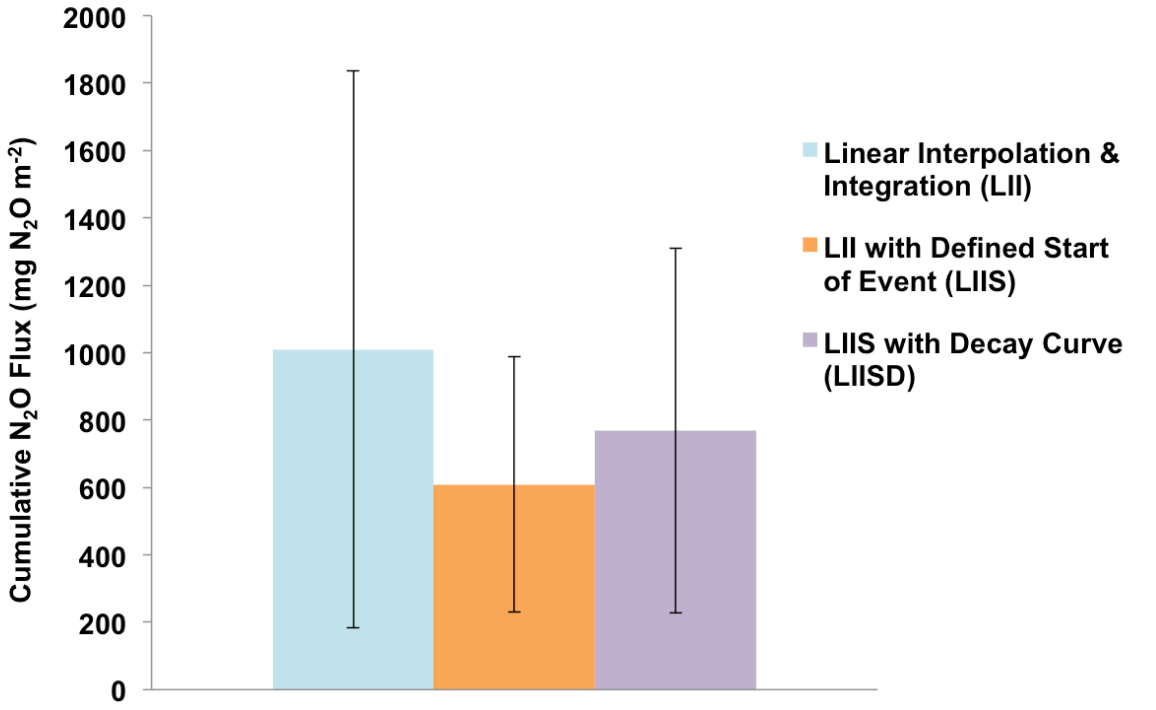

Figure 15. Cumulative N_2O flux derived from three different approaches: linear interpolation; linear interpolation with adjustment for start of the increase in N_2O emissions; and linear interpolation with adjustment for start of the increase in N_2O emissions combined with an exponential decay curve to describe the peak in N_2O emissions. The error bars are one standard deviation for n = 4 sampling positions.

The lowest cumulative N_2O flux value (609 ± 379 mg N_2O m^{-2}) was derived by assuming a start time for the peak in N_2O emissions associated with the passage of tropical storm Ana and adjusting the linear interpolation between non-steady state static chamber measurements accordingly (LIIS). The absolute magnitude of the cumulative N_2O flux using the third approach (LIISD; 768 ± 540 mg N_2O m^{-2}) of combining all the data from the two

different measurement techniques used in this study fell in between the results for the LII and LIIS approaches.

While the associated uncertainties for each value of cumulative N_2O flux precludes claiming absolute differences between the three techniques (Figure 15), the trend in the data is consistent with the inherent potential bias associated with the LII and LIIS approaches. In this study, applying only a simple linear interpolation between non-steady state static chamber measurements (LII) over-estimated the cumulative N_2O flux as revealed by the temporal pattern in actual N_2O emissions derived from using the simple flow-through chambers (Figure 10). Correcting the tendency to over-estimate flux using the simple linear interpolation method by adding in an estimate of the start in enhanced N_2O emissions (LIIS) led to an inherent under-estimation in flux because of the time lag between the start in enhanced N_2O emissions and the actual peak in N_2O emissions (Figure 10). This tendency to under-estimate cumulative flux using the LIIS approach, at least in this study, was corrected by approximating the area under curve following the exponential decline after the peak in N_2O emissions (LIISD; Figure 15).

Reported Trends in Peak N_2O Emissions Following Rain Events

Several studies have observed increased soil-to-atmosphere N_2O flux in response to increased soil moisture from precipitation following N fertilization (Smith and Dobbie, 2001; Choudhary et al., 2002; Bateman and Baggs, 2005; Drury et al., 2011; Venterea et al., 2011; Deng et al., 2015). We observed a similar trend, with the bulk of cumulative N_2O flux occurring as a result of one flux event in response to increased soil moisture following tropical storm Ana (Figure 6 &Figure 8). For the remainder of the season no peak fluxes

were observed, though low-levels of N_2O flux were detectable. In an incubation study (Beare et al., 2009), rewetting of dried soils resulted in N_2O emissions 95 to 150 times higher than emissions from soils that had been continuously kept wet. While we expected to see a similar response from the rewetting of dried soils from precipitation events after sidedress N application and during corn senescence in mid-August, the N_2O flux did not peak following either event (Figure 6). This is probably due to low soil moisture as a result of below-average cumulative rainfall during the study period. From April 24 to September 3, 2015 (DOY 114 to 246) precipitation was ~ 100 mm less than the multi-year average (Arguez et al., 2010).

Nitrous oxide is a microbial product of both nitrification and denitrification. Denitrification is typically the dominant soil N_2O production mechanism, and it requires anaerobic conditions, NO_3^- and NO_2^-, and electron donors from organic C compounds (Philippot et al., 2007). Water-filled pore space (WFPS) is a factor affecting soil oxic conditions and N_2O emissions (Ma et al., 2010; Deng et al., 2015). The WFPS threshold for N_2O production via denitrification varies and is typically between 60-70% (Sehy et al., 2003; Bateman and Baggs, 2005). Throughout the growing season there were only four instances where the WFPS was above 60%. For three of those instances, this threshold was reached for 10 minutes or less, with WFPS quickly dropping below the 60% threshold (Figure 16). The only time WFPS was above 60% for more than 10 minutes was on May 11, 2015 (DOY 131) from 6:10 to 7:10 AM. It is likely that the flux remained low after the peak flux following tropical storm Ana due to lack of anaerobic conditions caused by drought.

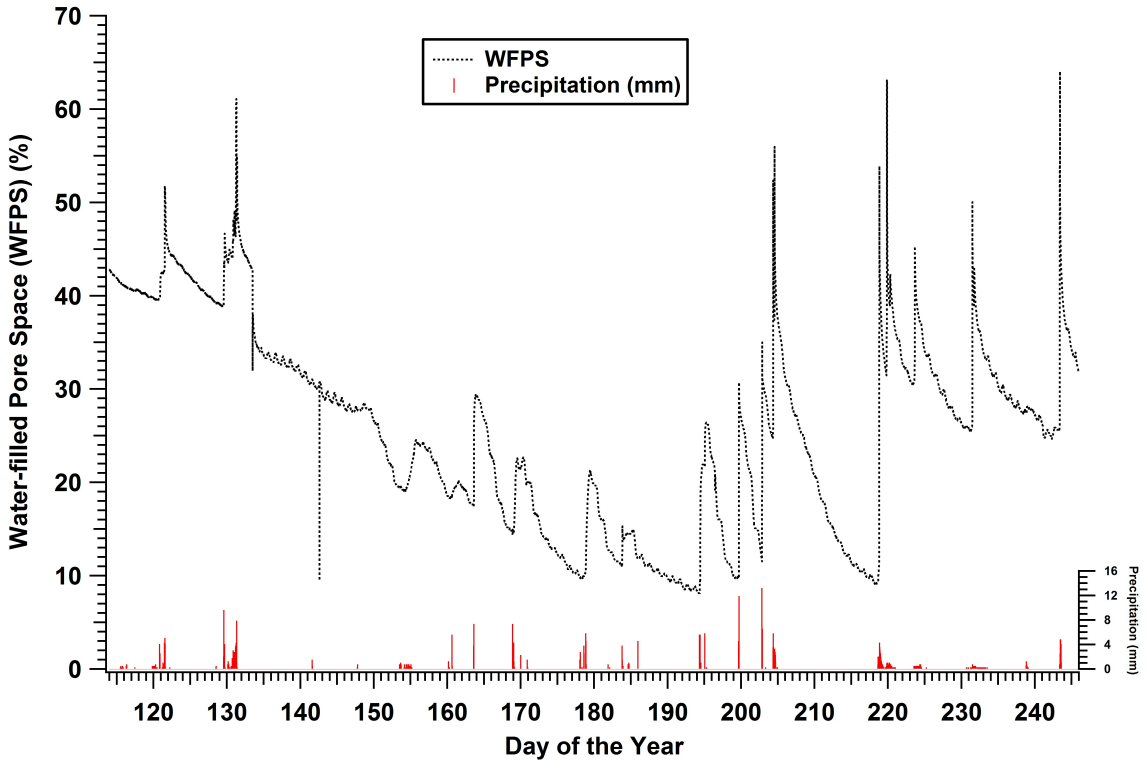

Figure 16. Water-filled pore space (WFPS) and precipitation from April 24 to September 23, 2015 (DOY 114 to 246). WFPS increased following precipitation and quickly decreased. The only instance where the 60% WFPS threshold for N_2O emissions occurred for more than 10 minutes was on May 11, 2015 (DOY 131) from 6:10 to 7:10 AM.

Our N_2O flux temporal curve differed from those of similar studies in conventional no-till fields during drought years. In Alabama, Smith et al. (2012) did not observe any peak flux in a field fertilized with broadcast-surface applied urea-ammonium nitrate, though consistent, low-level N_2O flux was detectable throughout the growing season. In Minnesota, maximum N_2O flux occurred following N fertilization, with peak fluxes continuing to be observed throughout the growing season, despite drought conditions (Venterea et al., 2011). In a field fertilized with urea, N_2O flux only occurred in late September, when precipitation frequency and magnitude increased after a summer drought (Drury et al., 2011). In the same study very low levels of flux were detectable throughout the season. While we observed one

peak flux event following N fertilization, we cannot say whether this trend will be repeated in the future.

Studies comparing flux from continuous monitoring systems with flux from non-steady state static chamber methods typically use a subset of the continuous data to represent manual sampling, rather than actually manually sampling (Parkin, 2008; Fassbinder et al., 2013). Smith and Dobbie (2001) measured flux with both a continuous flow-through system and non-steady state static chambers. Continuous flux measurements revealed temporal variation in emissions not detected by measurements from static chamber measurements made at 3-7 day intervals. While the absolute magnitude of the flux from the two chamber methods differed, the temporal patterns of N_2O flux were in agreement between the methods. Weitz et al. (1999) observed agreement between temporal N_2O emissions curves generated by continuous and non-steady state static chamber methods, with cumulative flux estimates from continuous measurements 14% greater than from static chamber measurements. Both Smith and Dobbie and Weitz et al. attributed the difference in the magnitude of flux between the methods to spatial variability. The agreement of the relative flux magnitude between the two methods in the study by Smith and Dobbie and Weitz et al. suggests it may be possible to modify our continuous system to quantitatively measure flux within the range measured by non-steady state static chamber methods.

Our flux values were higher than cumulative flux from similar studies (**Error! Reference source not found.**). Our RSD values were between 62.2 – 81.9%, with one chamber group emitting flux at higher rates than the remaining three chamber groups (Table 3). Thus, cumulative fluxes from 3/4 of our chamber groups were similar to the cumulative

values presented in**Error! Reference source not found.**. The reason why one chamber group emitted higher flux is unknown. However, it has been suggested that labile N availability, topographic depressions in the field, or the existence of denitrification "hot spots" could lead to increases in N_2O emissions at distances of a few meters (Hénault et al., 2012).

Table 3. Cumulative N_2O flux (mg m^{-2} h^{-1}) by static chamber group. Static chamber cumulative flux was calculated three ways: linear interpolation and integration (LII), LII with the start of the flux event defined (LIIS), and LIIS with a decay curve derived from continuous data and applied to static chamber data (LIISD).

	Cumulative N_2O Flux (mg m^{-2} h^{-1})		
Chamber Group	**Linear Interpolation & Integration (LII)**	**LII with Defined Start of Flux Event (LIIS)**	**LIIS with Decay Curve (LIISD)**
1	2219	1154	1546
2	861	572	715
3	517	400	462
4	440	310	350

Improvements to the system

We have shown that recording the temporal N_2O emissions curve with a continuous flow-through system and using it to calculate a simple model of decay can be used with non-steady state static chamber flux measurements to derive a closer approximation of flux, within the limits of inherent spatial variability at a research site. What we don't know is how this will work with successive peaks during the season, nor to what extent "fine structure" in temporal patterns reflects actual changes in soil emissions. In a season with multiple peaks, continuously monitoring the temporal emissions curve will reveal if there is consistency in both the timing of the peak after a rain event and in the rate of decay following the peak. Investigation of the "fine structure" in temporal patterns will determine whether these

fluctuations are affecting cumulative estimates of N_2O flux from static chamber measurements.

The continuous chambers remained in place during both sampling and standby mode. While the flow-through chambers were moved to new anchors as soon as possible after rain events, the extent to which the flow-through chambers altered the environment inside the chamber, and thus the production and flux of N_2O, is unknown. Automated chambers that cover the soil only long enough to take a sample multiple times a day would potentially reduce or eliminate the environmental effects that are due to the chamber being left in place, and would allow sunlight and precipitation to reach the soil when in standby mode. Further, by combining automated chambers with the ability to accurately measure flux continuously, the data can be subsampled in a similar way as Smith and Dobbie (2001) to prescribe sampling protocols for static chamber methods. These protocol recommendations can potentially minimize over or underestimation due to inaccurately accounting for the temporal pattern of N_2O flux. This continuous temporal data coupled with flux measured by the non-steady state static chamber technique is necessary for assessing the efficacy of and for making improvements to the current best practices for non-steady state static chamber sampling in the Southeast.

Table 4. Cumulative N_2O flux using non-steady state static chambers in no-till, corn systems fertilized with urea.

Author	Location	Dates	Frequency of Sampling	Event Flux Calculation Method	Cumulative Flux Calculation Method	Cumulative Flux (mg N_2O m^{-2})
(Omonode et al., 2011)	Missouri	4/8/05 – 9/13/05	Weekly, except for July during which only one measurement was made	Unknown	Linear interpolation and integration	364.24*
(Smith et al., 2012)	Alabama	4/9/07 – 8/6/07	0, 1, 2, 3, 4, 5, 14, 21, 31, 62, and 92 days after fertilization	Linear or curvilinear	Multiplied average flux value by total study time	1.26*
(Drury et al., 2011)	Ontario	5/1/05 – 10/31/05	Frequency of the 21 measurements is not stated	Linear	Linear interpolation and integration	248.06*
(Halvorson and Del Grosso, 2012)	Colorado	5/6/11 – 9/29/11	2 to 3 times per week	Linear or HM	Linear interpolation and integration	198.90
(Nash et al., 2012)	Missouri	4/23/09 – 8/28/09	3 to 4 times per week for 77 days after fertilization, then weekly	Linear or HM	Multiplied average flux value by total study time	714.35
Ross et al.	North Carolina	4/24/15 – 9/3/15	For 3 consecutive days following major rain events	Linear or HMR	Linear interpolation and integration	1009.43*
Ross et al.	North Carolina	4/24/15 – 9/3/15	For 3 consecutive days following major rain events	Linear or HMR	Linear interpolation and integration with defined start of event	608.86*
Ross et al.	North Carolina	4/24/15 – 9/3/15	For 3 consecutive days following major rain events	Linear or HMR	Linear interpolation and integration with defined start of event & peak flux estimate	768.15*

***indicates drought**

References

Arguez, A., Durre, I., Applequist, S., Squires, M., Vose, R., Yin, X., 2010. NOAA's U.S. Climate Normals (1981-2010) [WWW Document]. NOAA National Centers for Environmental Information. URL https://www.ncdc.noaa.gov/cdo-web/datatools/normals

Bateman, E.J., Baggs, E.M., 2005. Contributions of nitrification and denitrification to N_2O emissions from soils at different water-filled pore space. Biology and Fertility of Soils 41, 379–388.

Beare, M.H., Gregorich, E.G., St-Georges, P., 2009. Compaction effects on CO_2 and N2O production during drying and rewetting of soil. Soil Biology and Biochemistry 41, 611–621.

Bell, M.C., Raczkowski, C.W., 2008. Soil property indices for assessing short-term changes in soil quality. Renewable Agriculture and Food Systems 23, 70–79.

Chadwick, D.R., Cardenas, L., Misselbrook, T.H., Smith, K. a., Rees, R.M., Watson, C.J., McGeough, K.L., Williams, J.R., Cloy, J.M., Thorman, R.E., Dhanoa, M.S., 2014. Optimizing chamber methods for measuring nitrous oxide emissions from plot-based agricultural experiments. European Journal of Soil Science 65, 295–307.

Choudhary, M., Akramkhanov, A., Saggar, S., 2002. Nitrous oxide emissions from a New Zealand cropped soil: tillage effects, spatial and seasonal variability. Agriculture, Ecosystems & Environment 93, 33–43.

de Klein, C., Harvey, M., 2015. Nitrous Oxide Chamber Methodology Guidelines. Ministry for Primary Industries, Wellington, New Zealand.

Deng, Q., Hui, D., Wang, J., Iwuozo, S., Yu, C.-L., Jima, T., Smart, D., Reddy, C., Dennis, S., 2015. Corn Yield and Soil Nitrous Oxide Emission under Different Fertilizer and Soil Management: A Three-Year Field Experiment in Middle Tennessee. Plos One 10.

Drury, C.F., Reynolds, W.D., Yang, X.M., McLaughlin, N.B., Welacky, T.W., Calder, W., Grant, C.A., 2011. Nitrogen Source, Application Time, and Tillage Effects on Soil Nitrous Oxide Emissions and Corn Grain Yields. Soil Science Society of America Journal 76, 1268.

Fassbinder, J.J., Schultz, N.M., Baker, J.M., Griffis, T.J., 2013. Automated, low-power chamber system for measuring nitrous oxide emissions. Journal of Environmental Quality 42, 606–14.

Galloway, J.N., 2003. The Global Nitrogen Cycle, in: Treatise on Geochemistry. Elsevier Ltd., pp. 557–583.

Halvorson, A.D., Del Grosso, S.J., 2012. Nitrogen source and placement effects on soil nitrous oxide emissions from no-till corn. Journal of Environmental Quality 41, 1349–60.

Hénault, C., Grossel, A., Mary, B., Roussel, M., Léonard, J., 2012. Nitrous Oxide Emission by Agricultural Soils: A Review of Spatial and Temporal Variability for Mitigation. Pedosphere 22, 426–433.

Hutchinson, G., Mosier, A., 1981. Improved soil cover method for field measurement of nitrous oxide fluxes. Soil Science Society of America Journal 45, 311–316.

Hutchinson, G.L., Livingston, G.P., 2001. Vents and seals in non-steady-state chambers used for measuring gas exchange between soil and the atmosphere. European Journal of Soil Science 52, 675–682.
IPCC, 2007. Climate Change 2007: The Physical Science Basis. Contribution of Working Group I to the Fourth Assessment Report of the Intergovernmental Panel on Climate Change. Cambridge University Press, Cambridge, United Kingdom and New York, NY, USA.
Livingston, G.P., Hutchinson, G.L., Spartalian, K., 2006. Trace Gas Emission in Chambers. Soil Science Society of America Journal 70, 1459.
Ma, B.L., Wu, T.Y., Tremblay, N., Deen, W., Morrison, M.J., Mclaughlin, N.B., Gregorich, E.G., Stewart, G., 2010. Nitrous oxide fluxes from corn fields: on-farm assessment of the amount and timing of nitrogen fertilizer. Global Change Biology 16, 156–170.
Nash, P.R., Motavalli, P.P., Nelson, K. a., 2012. Nitrous Oxide Emissions from Claypan Soils Due to Nitrogen Fertilizer Source and Tillage/Fertilizer Placement Practices. Soil Science Society of America Journal 76, 983.
Oenema, O., Velthof, G.L., Yamulki, S., Jarvis, S.C., 1997. Nitrous oxide emissions from grazed grassland. Soil Use and Management 13, 288–295.
Omonode, R. a., Smith, D.R., Gál, A., Vyn, T.J., 2011. Soil Nitrous Oxide Emissions in Corn following Three Decades of Tillage and Rotation Treatments. Soil Science Society of America Journal 75, 152.
Parkin, T.B., 2008. Effect of sampling frequency on estimates of cumulative nitrous oxide emissions. Journal of Environmental Quality 37, 1390–5.
Parkin, T.B., Venterea, R.T., 2010. Chamber-Based Trace Gas Flux Measurements, in: Follett, R.. (Ed.), Sampling Protocols. pp. 3–1 to 3–39.
Pedersen, A.R., Petersen, S.O., Schelde, K., 2010. A comprehensive approach to soil-atmosphere trace-gas flux estimation with static chambers. European Journal of Soil Science 61, 888–902.
Philippot, L., Hallin, S., Schloter, M., 2007. Ecology of Denitrifying Prokaryotes in Agricultural Soil, in: Advances In Agronomy. Elsevier Inc., pp. 249–305.
Reeves, S., Wang, W., 2015. Optimum sampling time and frequency for measuring N_2O emissions from a rain-fed cereal cropping system. Science of The Total Environment 530-531, 219–226.
Rochette, P., Eriksen-Hamel, N.S., 2008. Chamber Measurements of Soil Nitrous Oxide Flux: Are Absolute Values Reliable? Soil Science Society of America Journal 72, 331.
Sehy, U., Ruser, R., Munch, J.C., 2003. Nitrous oxide fluxes from maize fields: Relationship to yield, site-specific fertilization, and soil conditions. Agriculture, Ecosystems and Environment 99, 97–111.
Smith, K. a., Dobbie, K., 2001. The impact of sampling frequency and sampling times on chamber-based measurements of N_2O emissions from fertilized soils. Global Change Biology 7, 933–945.
Smith, K., Watts, D., Way, T., Torbert, H., Prior, S., 2012. Impact of Tillage and Fertilizer Application Method on Gas Emissions in a Corn Cropping System. Pedosphere 22, 604–615.

Soil Survey Staff, Natural Resources Conservation Service, United States Department of Agriculture, 2015. Web Soil Survey [WWW Document]. URL http://websoilsurvey.nrcs.usda.gov/

USEPA, 2013. Inventory of U.S. Greenhouse Gas Emissions and Sinks: 1990-2011. Washington, DC.

Velthof, G.L., Jarvis, S.C., Stein, A., Allen, a. G., Oenema, O., 1996. Spatial variability of nitrous oxide fluxes in mown and grazed grasslands on a poorly drained clay soil. Soil Biology and Biochemistry 28, 1215–1225.

Venterea, R.T., 2010. Simplified Method for Quantifying Theoretical Underestimation of Chamber-Based Trace Gas Fluxes. Journal of Environmental Quality 39, 126–135.

Venterea, R.T., Bijesh, M., Dolan, M.S., 2011. Fertilizer source and tillage effects on yield-scaled nitrous oxide emissions in a corn cropping system. Journal of Environmental Quality 40, 1521–31.

Wagner, S.W., Reicosky, D.C., Alessi, R.S., 1997. Regression models for calculating gas fluxes measured with a closed chamber. Agronomy Journal 89, 279–284.

Weitz, A.M., Keller, M., Linder, E., Crill, P.M., 1999. Spatial and temporal variability of nitrogen oxide and methane fluxes from a fertilized tree plantation in Costa Rica. Journal of Geophysical Research-Atmospheres 104, 30097–30107.

APPENDIX

Appendix A

Final Static Chamber N_2O Flux Calculations

Table A 1. Final nitrous oxide flux calculations from CEFS determined by the HMR method or linear regression. Flux values were used in analyses in Chapter 2. Flux was measured at ~ noon each day.

Day of Year	Date	Chamber Group Number	Method	Flux (mg N_2O m^{-2} h^{-1})
120	4/30/15	1	HMR	0.7670
120	4/30/15	4	HMR	0.0436
120	4/30/15	3	HMR	0.0601
120	4/30/15	2	LR	0.0570
126	5/6/15	4	HMR	0.1616
126	5/6/15	3	LR	0.8618
126	5/6/15	2	HMR	0.5022
126	5/6/15	1	LR	0.9618
132	5/12/15	1	HAND	18.7199
132	5/12/15	2	HMR	2.4491
132	5/12/15	4	HMR	2.3315
132	5/12/15	3	LR	5.6914
133	5/13/15	1	LR	9.0434
133	5/13/15	2	LR	0.3886
133	5/13/15	4	HMR	0.9838
133	5/13/15	3	LR	1.2266
134	5/14/15	1	LR	1.9351
134	5/14/15	2	LR	0.2952
134	5/14/15	4	LR	0.6017
134	5/14/15	3	LR	0.7631
135	5/15/15	1	LR	0.9399
135	5/15/15	2	LR	0.4149
135	5/15/15	4	LR	0.3562
135	5/15/15	3	LR	0.4991
140	5/20/15	1	HMR	0.3076
140	5/20/15	3	HMR	0.2164

140	5/20/15	2	LR	0.2894
140	5/20/15	4	LR	0.2615
142	5/22/15	1	LR	0.0969
142	5/22/15	3	HMR	0.0877
142	5/22/15	2	LR	0.2475
142	5/22/15	4	LR	0.1360
148	5/28/15	1	LR	0.0407
148	5/28/15	2	HMR	0.1006
148	5/28/15	4	LR	0.1093
148	5/28/15	3	HMR	0.0752
156	6/5/15	1	LR	0.0467
156	6/5/15	2	HMR	0.1116
156	6/5/15	4	HMR	0.1684
156	6/5/15	3	HMR	0.2197
161	6/10/15	2	HMR	0.1896
161	6/10/15	4	HMR	0.0655
161	6/10/15	3	HMR	0.0559
161	6/10/15	1	HMR	0.0543
162	6/11/15	2	HMR	0.1248
162	6/11/15	4	HMR	0.0554
162	6/11/15	3	HMR	0.0503
162	6/11/15	1	HMR	0.0314
167	6/16/15	2	HMR	0.0407
167	6/16/15	4	LR	0.0288
167	6/16/15	3	HMR	0.0319
167	6/16/15	1	LR	0.0205
180	6/29/15	2	LR	0.0361
180	6/29/15	4	LR	0.0303
180	6/29/15	3	HMR	0.0279
180	6/29/15	1	HMR	0.0314
194	7/13/15	1	HMR	0.0612
194	7/13/15	2	HMR	0.0672
194	7/13/15	4	LR	0.0585
194	7/13/15	3	HMR	0.0473

196	7/15/15	1	HMR	0.0309
196	7/15/15	2	HMR	0.0402
196	7/15/15	4	HMR	0.0311
196	7/15/15	3	HMR	0.0351
201	7/20/15	2	LR	0.0315
201	7/20/15	4	HMR	0.0248
201	7/20/15	3	LR	0.0362
201	7/20/15	1	HMR	0.0362
204	7/23/15	2	LR	0.0465
204	7/23/15	4	LR	0.0408
204	7/23/15	3	HMR	0.0641
204	7/23/15	1	LR	0.0293
205	7/24/15	2	HMR	0.0603
205	7/24/15	4	LR	0.0920
205	7/24/15	3	HMR	0.2474
205	7/24/15	1	HMR	0.0360
206	7/25/15	2	HMR	0.0433
206	7/25/15	4	LR	0.0448
206	7/25/15	3	HMR	0.0679
206	7/25/15	1	HMR	0.0318
207	7/26/15	2	LR	0.0349
207	7/26/15	4	HMR	0.0355
207	7/26/15	3	HMR	0.0565
207	7/26/15	1	LR	0.0254
211	7/30/15	2	LR	0.0160
211	7/30/15	4	LR	0.0113
211	7/30/15	3	HMR	0.0132
211	7/30/15	1	LR	0.0119
219	8/7/15	2	HMR	0.0478
219	8/7/15	4	LR	0.0257
219	8/7/15	3	LR	0.0743
219	8/7/15	1	HMR	0.0427
220	8/8/15	2	LR	0.0519
220	8/8/15	4	HMR	0.0762

220	8/8/15	3	HMR	0.2399
220	8/8/15	1	LR	0.0650
221	8/9/15	2	HMR	0.0357
221	8/9/15	4	LR	0.0345
221	8/9/15	3	HMR	0.1001
221	8/9/15	1	LR	0.0420
232	8/20/15	2	HMR	0.0832
232	8/20/15	4	LR	0.0474
232	8/20/15	3	HMR	0.0455
232	8/20/15	1	HMR	0.0421
233	8/21/15	2	HMR	0.0575
233	8/21/15	4	LR	0.0270
233	8/21/15	3	LR	0.0155
233	8/21/15	1	HMR	0.0285
238	8/26/15	2	LR	0.0135
238	8/26/15	4	HMR	0.0252
238	8/26/15	3	HMR	0.0162
238	8/26/15	1	LR	0.0098
245	9/2/15	1	HMR	0.0401
245	9/2/15	2	HMR	0.0436
245	9/2/15	4	LR	0.0208
245	9/2/15	3	HMR	0.0402
246	9/3/15	1	HMR	0.1648
246	9/3/15	2	LR	0.0610
246	9/3/15	4	HMR	0.0695
246	9/3/15	3	HMR	0.0537

Appendix B

GC Standard Curves

Data for all the standard curves were fitted using a quadratic (second-order polynomial curve) model via IGOR Pro® software (WaveMetrics, Inc.). The resulting quadratic models were used to determine the concentration of N_2O in the exposed glass vials (see Appendix A).

Individual concentrations used to derive the multi-point calibration curves were prepared using zero grade air and a NIST-traceable certified N_2O stock calibration standard (~ 50 ppmv N_2O; Airgas®) in combination with a Teledyne® model T700 gas dilutor (Teledyne Advanced Pollution Instrumentation). The outlet from the Teledyne model T700 unit was connected to a Nylon manifold equipped with a septum for sampling. Output from the manifold was connected to 30.5 m of reinforced PVC tubing to prevent contamination of the standards by backflow of ambient air into the manifold during collection. The dilutor was operated for approximately 10 minutes at each selected concentration to ensure that the manifold-tubing combination was at equilibrium with the desired N_2O concentration. The use of the manifold allowed aliquots of the desired standard N_2O concentration to be obtained using either syringes equipped with valves or evacuated glass serum bottles. These in turn were immediately injected into the gas chromatograph following collection.

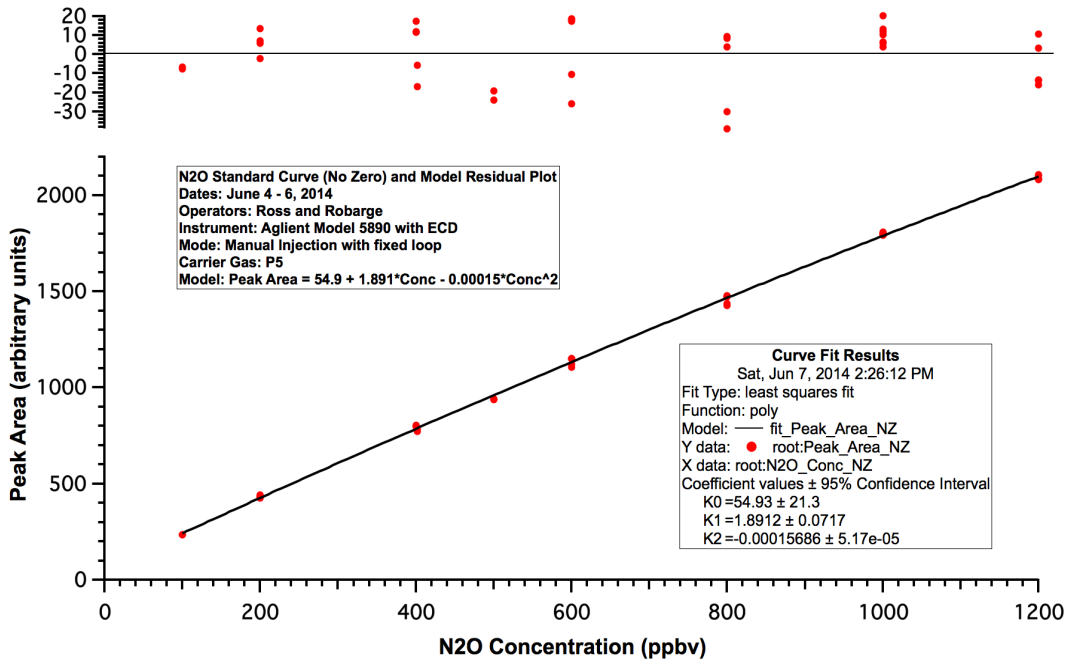

Figure B 1. Standard curve for static-chamber flux measurements made between 7 June and 29 July 2014. At the top of the figure is the residual standard deviation (RSD) showing how close the observed values are to the expected concentration values.

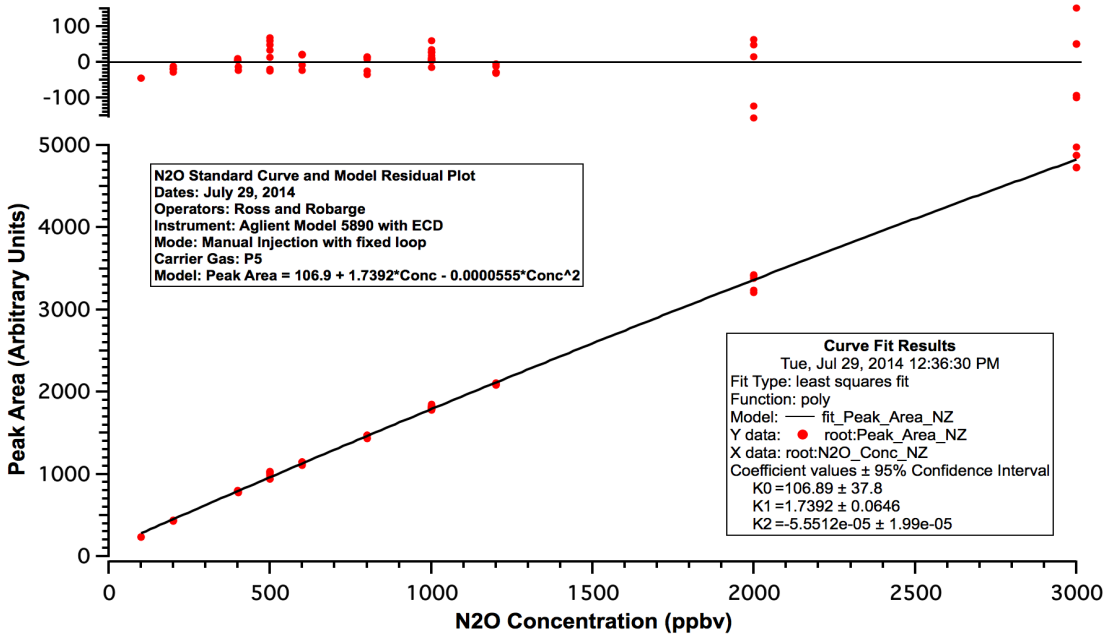

Figure B 2. Standard curve for static-chamber flux measurements made between 29 July and 31 October 2014. At the top of the figure is the residual standard deviation (RSD) showing how close the observed values are to the expected concentration values.

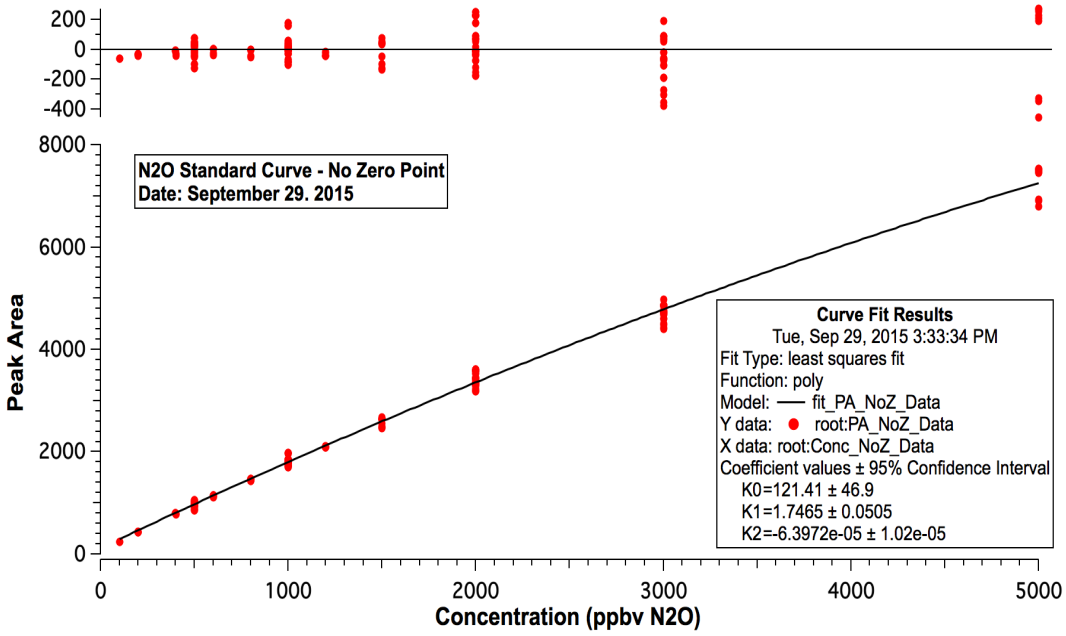

Figure B 3. Standard curve for measurements made between 20 April and 3 September 2015. At the top of the figure is the residual standard deviation (RSD) showing how close the observed values are to the expected concentration values.

Appendix C

Septa Holding Time Test

Objective
To assess the retention of gas using glass vials and red rubber septa for manual static chamber sampling.

Protocol

Treatments:
0 hours after filling - control
~24 hours after filling
~48 hours after filling
~72 hours after filling

Reps:
n = 10

Supplies:
- 40 100 ml glass serum vials
- 40 12.5-mm inner-diameter red rubber Suba-Seal® septa (Sigma-Aldrich Biotechnology LP)
- 2 two-way needles
- Vacuum with vacuum hose
- Timer
- Dilutor hooked up to zero air and N_2O with a manifold with a septum and ~100 feet of tubing to prevent ambient air backflow when collecting samples
- 1 60-ml Syringe with stopcock and needle

Steps:
1. Turn dilutor on to 2000 ppbv N_2O at 3.0 LPM (or your desired target concentration and flow rate) and start timer.
2. After ~5 minutes use the syringe and needle to extract ~60 ml of gas from the manifold. Release gas into ambient air in room.
3. Reinsert needle into manifold. Extract ~30 ml gas and, keeping the needle in the manifold, release gas back into manifold.
4. Keeping syringe in the manifold, let gas flow for ~10 seconds and extract 30 ml of gas.
    a. Tighten stopcock
    b. Remove needle from manifold
5. Immediately inject 5-10ml of gas into GC. Record GC Area, height and file number.
6. Repeat steps 3 to 5 until GC readings have stabilized, ~5-6 times.

7. Close vial with 1 intact septum
8. Insert 1 two-way needle into vacuum hose, insert needle into septum in vial, and vacuum vial for 2 minutes. Remove vial, making sure not to let the needle come out of the vacuum hose.
9. Using 1 two-way needle inserted in the septum of the manifold connected to the dilutor, insert vacuumed vial onto other end of fill vial with known concentration of N_2O for 2 minutes
    a. Record the date and time filled
    b. Let the dilutor run ~3 minutes between vials
10. For Time 0 reps, run 5 ml of gas from vial on GC immediately and repeat steps 1 to 6.
    a. After starting each GC run, flush the line with a syringe full of ambient air.
    b. Record the time of GC run start, area, height, and file number.
11. For remaining reps, run 10 vials each day for 3 consecutive days
    a. After starting each GC run, flush the line with a syringe full of ambient air.
    b. Record the time of GC run start, area, height, and file number.

Results

Vial and septa N_2O concentrations are plotted as a function of time in Fig. C-1 and as a function of percent difference from 2000 ppbv N_2O in Fig. C-2. The N_2O concentrations for days 0, 1, 2, and 3 after filling were 1953 ± 31.7, 1962 ± 11.2, 1935 ± 27.6, and 2036 ± 56.4 ppbv N_2O, respectively (Table C-1). The average percent N_2O concentrations relative to 2000 ppbv for days 0 through 3 was 98.6 ± 2.2%. There were no differences in N_2O concentrations between days 0, 1, and 2. This suggests that there is an optimal 48-hour usage window following vacuuming for maximum gas retention when using glass serum vials with red rubber septa.

Table C 1. Average N_2O concentration in glass vials sealed with red septa presented as absolute values and as percent of 2000 ppbv N_2O over time. Vials (n=10) were filled with 2000 ppbv N_2O on day 0, and N_2O concentrations were measured for three consecutive days following filling. Values followed by different letters denotes difference at the p<0.01 level.

Date	Days Since Filling Vial	Average N_2O Concentration (ppbv)	Std. Dev.	% Conc. relative to 2000 ppbv	% RSD
2/1/16	0	1953[a]	31.7	97.7	1.62
2/2/16	1	1962[a]	11.2	98.1	0.57
2/3/16	2	1935[a]	27.6	96.8	1.43
2/4/16	3	2036[b]	56.4	101.8	2.77

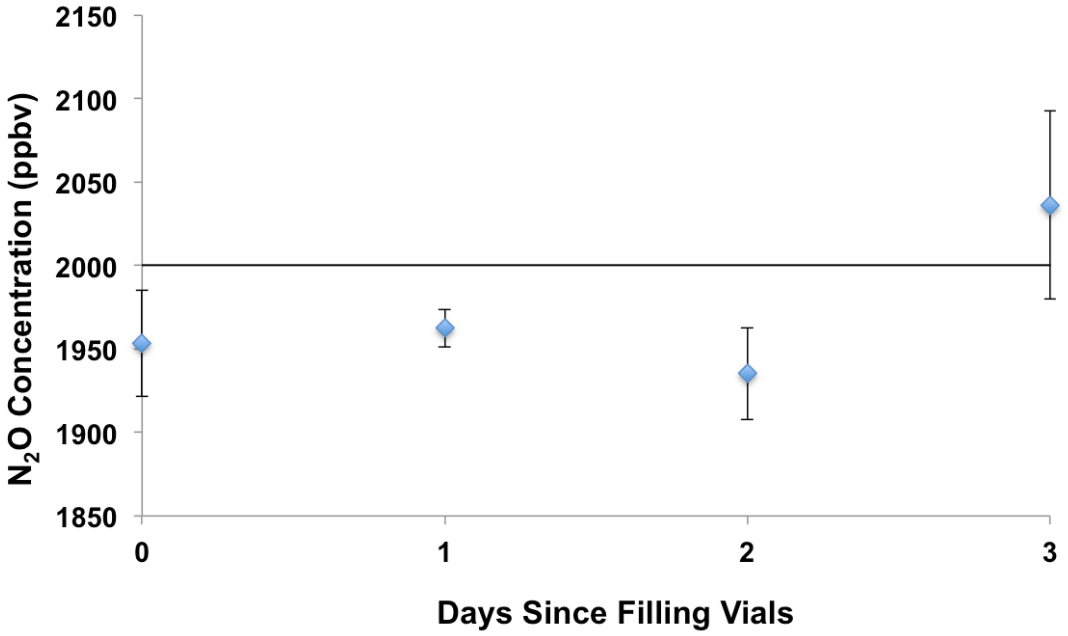

Figure C 1. Average N_2O concentration in glass vials sealed with red septa over time Average vials and red rubber septa versus time. Vials (n=10) were filled with 2000 ppbv N_2O on day 0, and the N_2O concentration was measured for three consecutive days following filling.

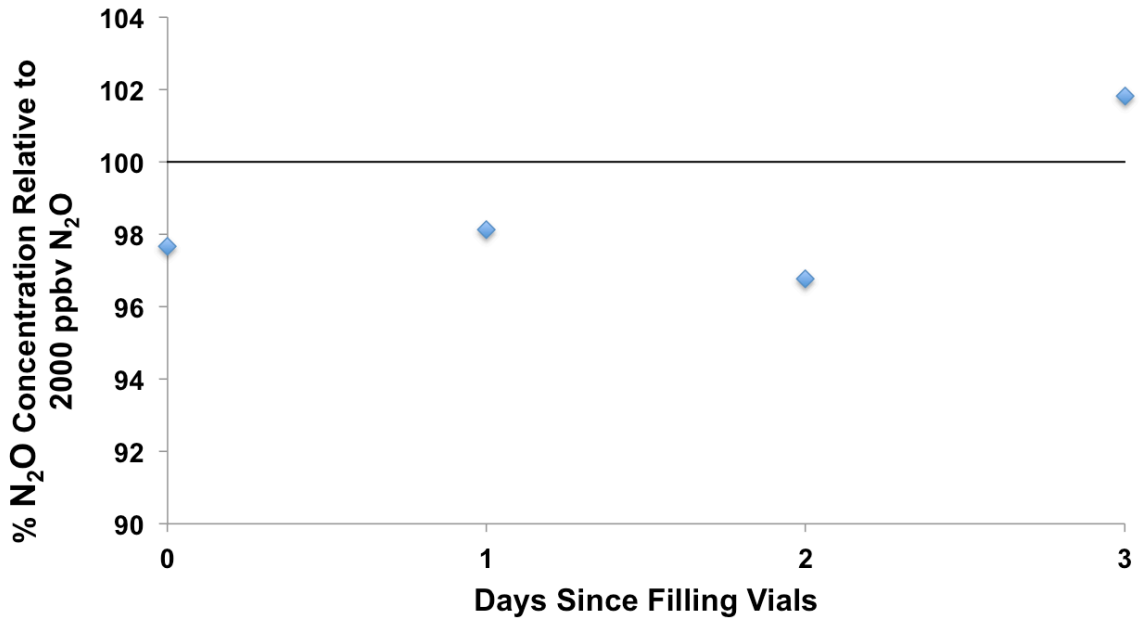

Figure C 2. Nitrous oxide concentrations in glass vials sealed with red rubber septa over time as a percent of 2000 ppbv N_2O. Vials (n=10) were filled with 2000 ppbv N_2O on day 0, and the N_2O concentration was measured for three consecutive days following filling.

Appendix D

Septa N_2O Sorption Test

Objective
To assess the extent of N_2O sorption by the glass vials and red rubber septa used for manual static chamber sampling in this study.

Protocol

Treatments:
0 hours after filling - control
~24 hours after filling
~48 hours after filling
~72 hours after filling

Reps:
n = 10

Supplies:
- 40 100 ml glass serum vials
- 80 12.5-mm inner-diameter red rubber Suba-Seal® septa (Sigma-Aldrich Biotechnology LP)
- 2 two-way needles
- Vacuum with vacuum hose
- Timer
- Dilutor hooked up to zero air and N_2O with a manifold with a septum and ~100 feet of tubing to prevent ambient air backflow when collecting samples
- Scissors or razor blade
- 1 60-ml Syringe with stopcock and needle

Steps:
12. Turn dilutor on to 2000 ppbv N_2O at 3.0 LPM (or your desired target concentration and flow rate) and start timer.
13. After ~5 minutes use the syringe and needle to extract ~60 ml of gas from the manifold. Release gas into ambient air in room.
14. Reinsert needle into manifold. Extract ~30 ml gas and, keeping the needle in the manifold, release gas back into manifold.
15. Keeping syringe in the manifold, let gas flow for ~10 seconds and extract 30 ml of gas.
    a. Tighten stopcock
    b. Remove needle from manifold
16. Immediately inject 5-10ml of gas into GC. Record GC Area, height and file number.

17. Repeat steps 3 to 5 until GC readings have stabilized, ~5-6 times.
18. Cut 1 septum in pieces small enough to put inside of and remove from vial
19. Insert 1 total chopped septum into 1 vial
20. Close vial with 1 intact septum
21. Insert 1 two-way needle into vacuum hose, insert needle into septum in vial, and vacuum vial for 2 minutes. Remove vial, making sure not to let the needle come out of the vacuum hose.
22. Using 1 two-way needle inserted in the septum of the manifold connected to the dilutor, insert vacuumed vial onto other end of fill vial with known concentration of N_2O for 2 minutes
    a. Record the date and time filled
    b. Let the dilutor run ~3 minutes between vials
23. For Time 0 reps, run 5 ml of gas from vial on GC immediately and repeat steps 1 to 6.
    a. After starting each GC run, flush the line with a syringe full of ambient air.
    b. Record the time of GC run start, area, height, and file number.
24. For remaining reps, run 10 vials each day for 3 consecutive days
    a. After starting each GC run, flush the line with a syringe full of ambient air.
    b. Record the time of GC run start, area, height, and file number.

Results

Septa N_2O sorption concentrations are plotted as a function of time in Fig. D-1 and as a function of percent difference from 2000 ppbv N_2O in Fig. D-2. The N_2O concentrations for days 0, 1, 2, and 3 after filling were 1963 ± 36.9, 1888 ± 35.3, 2032 ± 54.9, and 1920 ± 78.7 ppbv N_2O, respectively (Table D-1). The average percent N_2O concentrations relative to 2000 ppbv for days 0 through 3 was 97.5 ± 3.1%. There were no changes in N_2O concentrations in vials containing one dissected septum when compared to N_2O concentrations in vials without the presence of dissected septa (Appendix C). This suggests that the red rubber septa are neither sorbing nor releasing N_2O.

Table D 1. Concentration of N_2O in the presence of dissected red rubber septa expressed as absolute concentration and as percent of 2000 ppbv N_2O over time. Vials (n=10) were filled with 2000 ppbv N_2O and one dissected septum on day 0, and N_2O concentrations were measured for three consecutive days following filling. Values followed by different letters denotes difference at the $p<0.05$ level.

Date	Days Since Filling Vial	Average N_2O Concentration (ppbv)	St. Dev.	% Conc. relative to 2000 ppbv	% RSD
2/2/16	0	1963[a]	36.9	98.1	1.88
2/3/16	1	1888[b]	35.3	94.4	1.87
2/4/16	2	2032[c]	54.9	101.6	2.73
2/5/16	3	1920[ab]	78.7	96.0	4.10

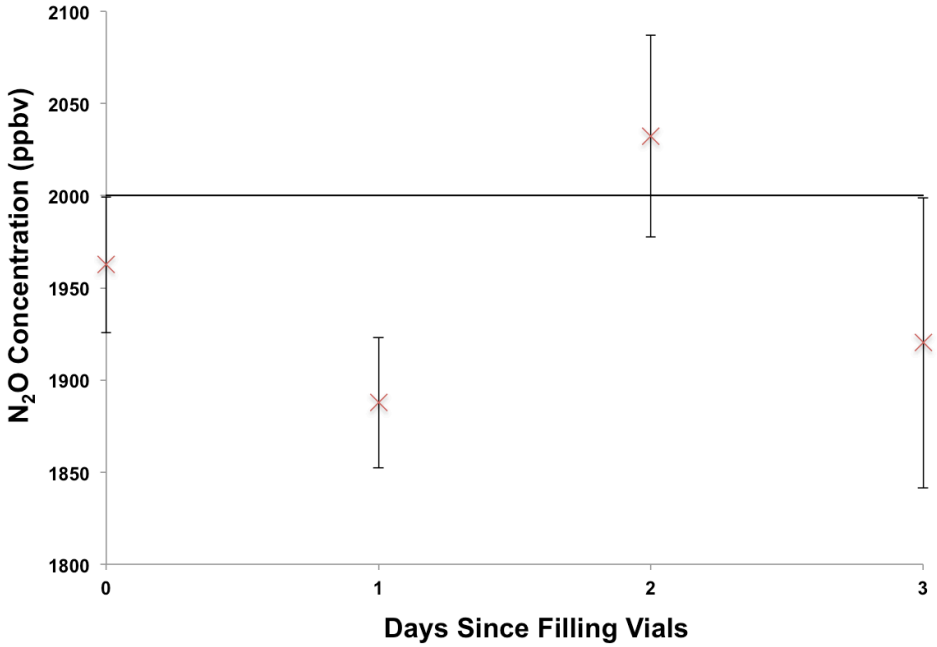

Figure D 1. Average N_2O concentrations by glass vials sealed with red rubber septa over time. Vials (n=10) were filled with 2000 ppbv N_2O and one dissected red rubber septum on day 0, and the N_2O concentration was measured for three consecutive days following filling.

Figure D 2. Average N_2O concentrations in glass vials sealed with red rubber septa over time as a percent of 2000 ppbv N_2O. Vials (n=10) were filled with 2000 ppbv N_2O and one dissected red rubber septum on day 0, and the N_2O concentration was measured for three consecutive days following filling.

Appendix E

Peak Flux Calculated from Derived Decay Curve

As discussed in Chapter 2, the simple flow-through chambers provided an index for the time of peak N_2O emissions on May 12, 2015 observed among the 4 group positions, as well as an index of the rate of decline in N_2O emissions (Fig. #). The decrease in peak N_2O emissions at each position sampled along the subplot was described using a simple exponential decay curve:

$$\text{Static Chamber } N_2O \text{ flux} = Ae^{(-Bx)} \qquad (2)$$

where x is time in hours, B is the decay constant, and A is the peak in N_2O flux. An estimate of the decay constant (B) was plotted using the linear form of Eq. 2 as the natural log of N_2O concentration measured with the simple flow-through chambers as a function of time relative to the observed peak in N_2O concentration (time equals zero hours). A linear regression was then fitted to the data. The estimate of the decay constant (B) was obtained from the slope of the fitted line.

Peak flux values (A) were then calculated using static chamber N_2O flux measurements taken 18.63 hours after the peak. An estimate of A was calculated using these static chamber flux measurements taken again at 42.63, 66.63 and 90.63 hours after the peak flux.

Results

The A values calculated using static chamber measurements taken at 18.63, 42,63, 66.63 and 90.63 hours after the peak are plotted in Fig. E 1 as a percent relative to the 18.63-hour A value. Absolute A values are given in Table E 1. The calculated A values ranged

from 2.0 to 46.5 mg N_2O m^{-2} h^{-1}. The calculated A values as a percent of the 18.63-hour A value ranged from 40% to 269%. In group 1 the A value first increased following the 18.63-hour A value. It then decreased and increased again. For groups 2 and 3, A values decreased at the 42.63-hour time point and then increased. For group 4, A values increased following the 18.63-hour A value. The maximum A value in group 1 resulted from using the 42.63-hour static chamber measurement to calculate peak emissions, while for groups 2, 3, and 4 the maximum A values resulted from using the 90.63-hour static chamber measurement.

Table E 1. Static chamber measurements were taken 18.63, 42.63, 66.63 and 90.63 hours after the peak emissions that occurred on May 12, 2015. Peak flux A-values were calculated using static-chamber measurements and the decay curve derived from continuous, flow-through measurements. A-values are shown here as absolute values and as a percent of the calculated A-value from static chamber measurements collected 18.63 hours after the peak. (Units = mg N_2O m^{-2} h^{-1})

Absolute A Values of Calculated Peak Emissions (mg N_2O m^{-2} h^{-1})						
Hours after peak	**18.63**	**42.63**	**66.63**	**90.63**	**Average**	**St. Dev.**
Group 1	38.3	46.5	25.0	30.5	35.1	9.4
Group 2	11.6	6.3	9.9	16.2	11.0	4.1
Group 3	5.0	2.0	3.8	13.5	6.1	5.1
Group 4	4.8	5.1	7.8	11.6	7.3	3.2

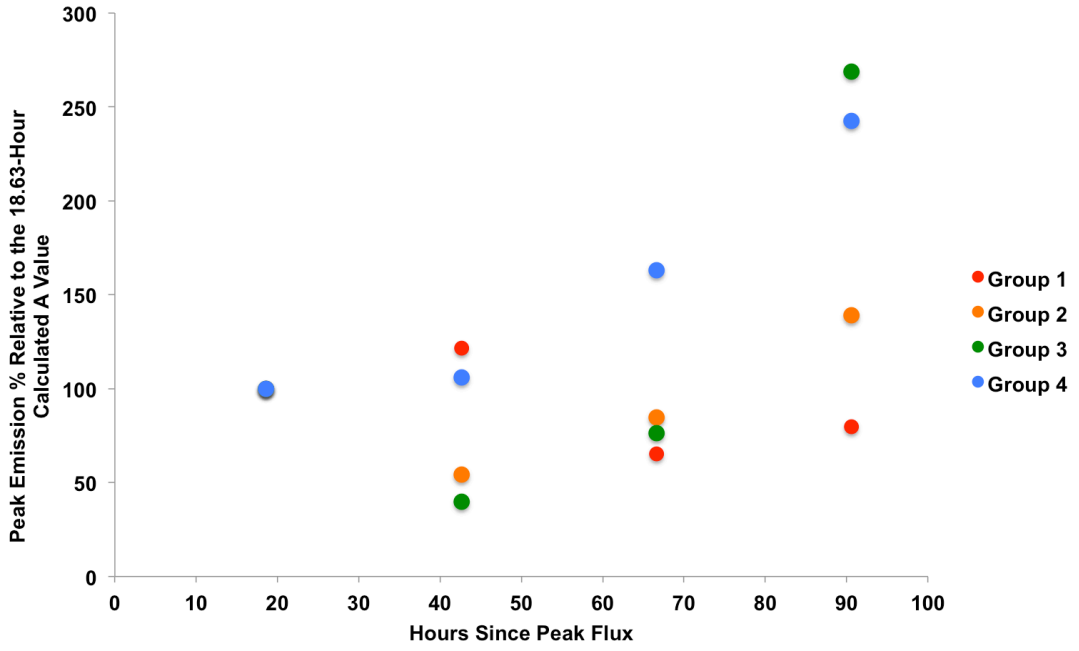

Figure E 1. Static chamber measurements were made 18.63, 42.63, 66.63 and 90.63 hours after the peak flux. Shown here are the peak flux values (A values) calculated using derived decay curve (Eq. 2) as a percent of the A value calculated using the static chamber measurements made 18.63 hours after the peak.

Discussion

To understand how static-chamber flux measurements and time since the peak affect the calculated A value, Eq. 2 was transformed into its linear form and solved for A expressed as ln (A):

$$\ln (A) = \ln (\text{static chamber } N_2O \text{ flux}) - (-Bx) \qquad (3)$$

where x is time since peak flux in hours, B is the decay constant (0.0384 ± 0.0047), and A is the peak in N_2O flux. When calculating ln (A) at 18.63 hours after the peak, greater weight is given to ln (static chamber N_2O flux) than to Bx for all groups. Greater weight is given to Bx for groups 2, 3, and 4 at 42.63 hours after the peak and for all groups at 66.63 and 90.63 hours after the peak. Except for when flux is very high, as time since peak increases, the magnitude of hours since the peak contributes more to the A value than does the static

chamber flux (Table E-2). We assumed when calculating A values using a derived decay constant, static chamber measurements taken closer to the peak generally provide more reliable A value estimates than those taken further in time from the peak.

Table E 2. Comparison of time since peak flux and static chamber flux measurements in calculating A values using Eq. 3.

		ln (static chamber N_2O flux)			
x	**-Bx**	**Group 1**	**Group 2**	**Group 3**	**Group 4**
18.63	-0.72	2.93	1.74	0.90	0.85
42.63	-1.64	2.20	0.20	-0.95	-0.02
66.63	-2.56	0.66	-0.27	-1.22	-0.51
90.63	-3.48	-0.06	-0.70	-0.88	-1.03

Appendix G

Python Code for Processing Continuous Concentration Data

```
# Program for Averaging N2O Continuous Data From Chambers
# Prepared By: Wayne Robarge
# Date: October 7, 2015
# Python ver. 3.5.0

# This program is designed for averaging continuous data for Ross Project

# Initialization of Needed Variables
SplPos = 1
# This value needs to be set to first sample location in data file
filtervalue = 310
# This variable detemines initial portion of monitoring period that will be ignored
# Setting of 310 means only last 4 minutes of readings are included in averaging
filtercount = 0
C = ","
E ="\n"
EOF = 9999
icount = 0
master_count = 0
Sum_N2OCONC = 0
# Sum_Time = 0.0
icount = int(icount)
filtervalue = int(filtervalue)
filtercount = int(filtercount)
master_count = int(master_count)
SplPos = int(SplPos)
Sum_N2OCONC = float(Sum_N2OCONC)
# Sum_Time = float(Sum_Time)

# Averaging is achieved by looping through file line by line and using test conditions
print("\nLooping through the file, line by line.")
# Example input and output text file names. Format can vary.
text_file_in = open("BASF_ROSS_201509131006_Average_Input.csv", "r")
text_file_out = open("BASF_ROSS_201509131006_Average_Output.txt" , "w")

for line in text_file_in:
    master_count += 1
#   print(master_count)
```

```
#   print(line) # Read in line from file
#   Split input string into assigned variables using comma delimiter
    DateTime, FracDOY, N2OCONC, SplLoc, Sequence = line.split(",")
#   Convert variables into proper format
#   DateTime, Sequence requires no conversion leave as string variable
    DateTime = str(DateTime)
    FracDOY = float(FracDOY)
    N2OCONC = float(N2OCONC)
    SplLoc = int(SplLoc)
    Sequence = str(Sequence)
#   End of conversion of varibles into proper format
#   Use If/Else test to average data within a location over a given time period within data file
#   Starting SplLoc value will have to be entered for each data file processed, see above
initialized values
#   Sum over parameters want to average within a given location
    if SplLoc == SplPos:
        icount += 1
        filtercount += 1
        Sum_N2OCONC += N2OCONC
        preDateTime = DateTime
        preSequence = Sequence
#   Use pre variables to retain last line inputs where SplLoc == SplPos test is true
#   Test condition to filter out first 6 minutes of reading at new loaction to avoid carry over
from previous location for gases
        if icount <= filtervalue:
            filtercount = 0
            Sum_N2OCONC = 0
        # then continue with original test condition
# When detect new location, calculate averages, reset with current location values and output
data
    else:
        if icount > filtervalue:
            Mean_N2OCONC = float(Sum_N2OCONC/filtercount)
#   Need to be sure to append new line character to avoid continuous string during WRITE
operation
            line =
preDateTime+C+str(FracDOY)+C+str(Mean_N2OCONC)+C+str(SplPos)+C+preSequence+
E
            print(master_count, icount, filtercount, line)
            text_file_out.write(line)
#       Sum_AmbT = AmbT
#   Reset counter for next location, and reset logic test to account for new line of input at next
sampling location
```

```
        icount = 1
        filtercount = 0 # this is index for gases and we do not include first reading from new
location
        SplPos = SplLoc
        Sum_N2OCONC = 0 # make sure there is no carryover between locations


text_file_in.close()
text_file_out.close()

#   input("\n\nPress the enter key to exit.")
```

Appendix H

Arduino Microprocessor Code

```
 /*
 Name: Valve Controller
 Owners: R.Austin, W.Robarge
 Produced: May 2014
 RE: Turn on 5 relays alternating for 30 minutes on
 EXAMPLE: we are running 4 chambers (A,B,C,D) and one Ambient location.
        The desired repeating pattern would be as follows:
        A, B, Ambient, C, D, Ambient, A, B, Ambient, C, D, Ambient, etc.
 NOTE: July 22 - the sequence requested is A,B,C,D,E in sequence for 30 minutes each
 Note: Variables with "fan" refer to valves.
*/

#include <SimpleTimer.h>


// the timer object
SimpleTimer timer;
unsigned long interval = 1000;          // 10 second
unsigned long seconds = 0;              // initilize the running number of seconds the program
has been running
//unsigned long fanInterval = 60 * 12;    // The time to keep a fan on (in seconds) - 12
minutes
unsigned long fanInterval = 60 * 30;    // The time to keep a fan on (in seconds) - 30 minutes
//unsigned long fanInterval = 5;          // 5 seconds
//int seq[6] = { 1, 2, 5, 3, 4, 5 };      // 1,2,3,4,5 correspond to relays A,B,C,D,E
int seq[6] = { 1, 2, 3, 4, 5 };      // 1,2,3,4,5 correspond to relays A,B,C,D,E
int currSeqPosition = 0;                // used to interate through the sequence


// the current relay that is turned on (i.e. A,B,C,D, or E (E is ambient) correspond to pins
12,11,10,9,8
int fanOn = seq[currSeqPosition];
int sizeOfSeq = sizeof(seq)/sizeof(seq[0]);    // calculate the number of elements in the
sequence


// Set the Pins that the fans are connected to.
int fanPin08 = 8;            // ambient chamber
int fanPin09 = 9;            // chamber D
```

```
int fanPin10 = 10;           // chamber C
int fanPin11 = 11;           // chamber B
int fanPin12 = 12;           // chamber A

// Set up the data logger on analog pin 3
int dlPin = 3;

void setup() {
   pinMode(fanPin08, OUTPUT);
   pinMode(fanPin09, OUTPUT);
   pinMode(fanPin10, OUTPUT);
   pinMode(fanPin11, OUTPUT);
   pinMode(fanPin12, OUTPUT);
   pinMode(dlPin, OUTPUT);
   //Serial.begin(9600);
   timer.setInterval(interval, count);
   turnFanOn(fanOn);
}

void loop() {
   timer.run();
}

// a function to be executed by the timer (1/sec)
void count() {
  //Serial.print("Sec: ");
  //Serial.println(seconds);
  seconds += 1;
  if(seconds >= fanInterval) {
    seconds -= fanInterval;
    nextFan();
  }
  //Serial.print("Uptime (s): ");
  //Serial.println(millis() / 1000);
}


// Turns on the next fan in the sequence
void nextFan() {
   currSeqPosition += 1;                  // Move the the next number in the sequence
   if (currSeqPosition >= sizeOfSeq-1) {      // check to see if you are at the end of the
sequence (NOTE add -1 July 22 esit)
     currSeqPosition = 0;                 // Set back to start of sequence
```

```
    }
    fanOn = seq[currSeqPosition];
    turnFanOn(fanOn);
}


// Turn on the next Fan
void turnFanOn(int& fan) {
   turnAllOff();
   if(fan == 1) {
      digitalWrite(fanPin12, LOW);   // turn Fan on pin 12 on by pulling low  [chamber A]
      analogWrite(dlPin, 40);
   }
   if(fan == 2) {
      digitalWrite(fanPin11, LOW);   // turn Fan on pin 11 on by pulling low  [chamber B]
      analogWrite(dlPin, 80);
  }
  if(fan == 3) {
      digitalWrite(fanPin10, LOW);   // turn Fan on pin 10 on by pulling low  [chamber C]
      analogWrite(dlPin, 120);
  }
  if(fan == 4) {
      digitalWrite(fanPin09, LOW);   // turn Fan on pin 9 on by pulling low  [chamber D]
      analogWrite(dlPin, 180);
  }
  if(fan == 5) {
      digitalWrite(fanPin08, LOW);   // turn Fan on pin 8 on by pulling low  [E - ambient]
      analogWrite(dlPin, 220);
  }
  printFanInfo();
}


// Turn all the fans off this means setting them all to high (+5v)
void turnAllOff() {
  digitalWrite(fanPin08, HIGH);
  digitalWrite(fanPin09, HIGH);
  digitalWrite(fanPin10, HIGH);
  digitalWrite(fanPin11, HIGH);
  digitalWrite(fanPin12, HIGH);
  //analogWrite(dlPin, 0);
}
```

```
void printFanInfo() {
  Serial.print("Fan: ");
  Serial.println(fanOn);
}
```

Appendix I

Chamber Field Groups

Figure I 1. Schematic layout of the chamber groups and trailer in Field 6 at CEFS in Goldsboro, NC. Group 1 is closest to the trailer in the most NE position, with Groups 2, 3, and 4 following the edge of field 6 in a SW direction from Group 1.